Gut bacteria gatekeep host-specific colonization of a commensal fungus that boosts type 2 immunity

Geongoo Han[1], Rebecca Yunker[1], Mohammad H. Hasan[1], Alex Bruce[1], Kellie Baldaro[1], Jessica Pacia[1], Owen Lockwood[1], Dana Magana Miralles[1], Nicholas N. Jarjour[2,3], Karthikeyani Chellappa[1], Shipra Vaishnava[1]*, Lalit K. Beura[1]*

[1] Molecular Microbiology & Immunology Department, Brown University, Providence, RI 02912, USA.

[2] Center for Immunology, University of Minnesota, Minneapolis, MN 55455, USA.

[3] Department of Laboratory Medicine and Pathology, University of Minnesota, Minneapolis, MN 55455, USA.

* Corresponding author: lalit_beura@brown.edu, shipra_vaishnava@brown.edu

Abstract

Throughout evolution, organisms have developed exclusive and mutually beneficial relationships with microbes in their natural environments. While these species-specific host-microbe interactions are well-documented for in case of commensal bacteria, similar relationships for commensal fungi remain largely unexplored. In this study, we screened the gut mycobiome of non-laboratory rodents, to find host-specific fungi. We identified *Kazachstania pintolopesii* as a dominant fungus in pet store mice across various geographical locations. This fungus stably colonized laboratory mice, outcompeted non-murine fungi, and persisted independently of gut bacteria without triggering conventional antifungal responses. Colonization by *K. pintolopesii* significantly increased intestinal macrophage populations, which was crucial in preventing systemic immune recognition. *K. pintolopesii* also induced intestinal type 2 immune responses, providing cross-kingdom protection against helminths in free-living mammals exposed to parasitic protozoa. Notably, *K. pintolopesii* strains from non-murine hosts failed to colonize laboratory mice with intact gut bacteria despite high genomic similarity. In gnotobiotic mice, these non-murine strains disrupted bacterial communities and their associated metabolomes, unlike the mouse strains. Our findings establish host exclusivity as a hallmark of fungal commensalism and reveal commensal bacteria as gatekeepers of species-specific fungal colonization and their immune interactions with the mammalian host.

Keywords

Kazachstania pintolopesii, commensal fungi, host adaptation, microbiome, cross-kingdom protection, type 2 immunity

Introduction

Commensal microorganisms are crucial for host immunity and have coevolved with their natural hosts, often exhibiting high species restriction. This phenomenon is observed across various life forms. In invertebrates, the Hawaiian bobtail squid depends on *Vibrio fischeri* for tissue development [1] while tsetse flies rely on *Wigglesworthia glossinidia* for fitness and reproduction [2]. Similarly, in mammals, gut immune cell maturation is driven by host-specific bacteria. Experiments have shown that human or rat gut bacteria introduced into germ-free mice are less effective at stimulating immune cell development compared to mouse-specific bacteria, highlighting the importance of host-adapted microbes in shaping host physiology [3]. A well-studied example of such exclusive host-microbe interaction is segmented filamentous bacteria (SFB), which colonize their hosts with remarkable species specificity, providing significant immune benefits to their adapted host while failing to colonize non-specific hosts [4-6]. While these exclusive interactions have been extensively studied for symbiotic bacteria, similar examples are lacking for other members of the gut microbiome, such as fungi, despite their emerging role in immune modulation as gut colonizers.

The mammalian gut houses a complex ecosystem of microbes, including bacteria, viruses, and fungi. However, our understanding of whether and how commensal fungi interact exclusively with their hosts is limited due to the lack of true commensal models that can stably colonize the mouse gut without causing inflammation or requiring immune suppression. Most research efforts have focused on *Candida albicans,* a gut commensal that is the main cause of opportunistic infections in humans. However, studying *C. albicans* commensalism in humans is somewhat limited because of technical and ethical challenges. As such introducing *C. albicans* to murine gut has emerged as a dominant

62 model system. But this approach often requires antibiotic treatment to maintain stable
63 colonization and, can induce inflammatory responses compromising interpretation [7-9].
64 Therefore, alternative commensal fungi that have coevolved with their natural host, are
65 needed to better understand fungal-host symbiosis.

66 Laboratory mice are typically raised in highly controlled, specific pathogen-free (SPF)
67 environments. These conditions, while beneficial for reducing variability in experimental
68 outcomes, result in mice with limited exposure to diverse microbial communities, including
69 fungi. This lack of exposure leads to an immunologically naive phenotype, which is far
70 removed from the natural immune system of free-living mammals [10-12]. The differences in
71 microbial exposure between laboratory, wild, and pet store mice present a unique
72 opportunity to identify and characterize potential commensal fungi that have co-evolved
73 with their murine hosts [13,14]. By incorporating naturally occurring commensal fungi into
74 laboratory settings, researchers can create models that better reflect the complex
75 microbial environment of humans and reveal novel interactions between diverse fungal
76 commensals and their natural host.

77 In this study, we sought to isolate and characterize commensal fungi from pet store
78 mice to elucidate their unique interactions with host. We identified *Kazachstania*
79 *pintolopesii* as the dominant fungal species in the gut of pet store mice across different
80 geographical locations. Through a series of *in vivo* experiments and multi-omics analyses,
81 we investigated the colonization dynamics, host immune responses, and functional
82 consequences of *K. pintolopesii* colonization in laboratory mice. By comparing strains
83 isolated from murine and non-murine hosts, we uncovered the importance of a finely-
84 tuned host-specific metabolic adaptation for successful gut colonization by *K. pintolopesii*.

This discovery marks the first documented instance of host exclusivity for a fungal commensal species, opening avenues for exploring how such interactions influence immune responses, microbial competition, and overall host physiology.

Results

K. pintolopesii is the dominant gut fungus in pet store mice

Specific pathogen-free laboratory mice are maintained in controlled environments, shielded from potential pathogen exposure and typically harbor microorganisms with limited diversity. In contrast, pet store mice live in large breeding colonies and are routinely exposed to rich varieties of microbes, including pathogenic bacteria, viruses, parasites, and fungi [10]. As an example of this, electron microscopic imaging of the gut epithelial surface of laboratory mice revealed no significant epithelium-attached microbes. In contrast, the epithelial surfaces of pet store mice harbored a number of microbial-like structures of varying shapes and sizes (~2-15 μm) (Fig. 1A). Therefore, we used pet store mice as source to screen for commensal murine fungi.

Using ribosomal RNA-based probes, we were able to find presence of fungal species among these epithelial-associated microbes in pet store mice, which are largely absent in laboratory mice (Fig.1B). Fungal burden in the feces of pet store mice was notably high (~10^7 CFU/g of feces), while no fungal populations were detected in the feces of laboratory mice in our facility (Fig. 1C). Fungal colonization was observed throughout the gastrointestinal tract of the pet store mice, from the duodenum to the feces, with the fungal burden progressively increasing toward the caudal end of the intestine indicating that pet store mice are heavily colonized with fungi throughout the gastrointestinal tract (Fig. 1D).

To identify the commensal fungal species in the murine gut, we cultured the gut contents of the pet store mice for 5 days at 30 °C and randomly picked 26 colonies from the plates. Sequencing of the internal transcribed spacer (ITS) region of these colonies revealed that all colonies are the same fungal species, *Kazachstania pintolopesii* (Fig.

112 S1A). The isolate appeared as a budding yeast and had an ellipsoidal shape with typical
113 yeast cell structures such as a thick cell wall, nucleus, vacuole, and mitochondria (Fig.
114 S1B and C). The isolate showed higher ITS sequence similarities with other *Kazachstania*
115 species and *Saccharomyces cerevisiae*, whereas lower similarities with *Candida* and
116 *Aspergillus* species (Fig. S1D). We also directly sequenced the ITS1 region of the gut
117 metagenome of pet store mice. Intriguingly, this culture-independent analysis also
118 showed that the intestines of pet store mice were predominantly colonized by a single
119 fungal species, *K. pintolopesii*, which accounted for over 99% of the total sequence reads
120 in both the luminal and mucosal regions of the small intestine and colon (Fig. 1E).

121 To determine whether this observation is specific to pet stores in a particular region
122 (Rhode Island), fecal samples were collected from pet store mice in other geographical
123 locations, including Midwest United States (Minnesota) and Southern United States
124 (Texas) (Fig. S1E). Higher fungal burden was observed across all regions (Fig. 1F), with
125 *K. pintolopesii* consistently identified as the predominant fungal species in the gut,
126 regardless of the region (Fig. 1G). These findings indicate that *K. pintolopesii* is not limited
127 to a specific geographical area but rather is a prevalent member of the mouse mycobiome
128 under non-laboratory setting. It colonizes the gastrointestinal tract extensively, achieving
129 high population levels both near the mucosal surface and within the intestinal lumen.

130 ***K. pintolopesii* stably colonizes laboratory mice irrespective of gut bacteria and**
131 **provides colonization resistance against non-murine fungi**

132 To test whether this fungal isolate from the pet store mice could colonize the intestines of
133 the laboratory mice, we orally administered the isolated *K. pintolopesii* to laboratory mice.
134 A high fungal burden (~10^7 CFU/g of feces) was observed in the feces following

135 colonization, and this level was maintained for 6 weeks (Fig. 2A). *K. pintolopesii* was
136 located closely to the gut epithelium of mice, co-localizing with bacteria, similar to the
137 colonization pattern observed in the pet store mice (Fig. 2B).

138 We performed 16S rRNA gene sequencing to assess the impact of *K. pintolopesii*
139 colonization on the bacterial community in the gut. *K. pintolopesii* colonization maintained
140 bacterial community diversity, composition, and load without significant alterations (Fig.
141 2C - F).

142 Germ-free (GF) mice showed *K. pintolopesii* fecal colonization levels (~10^7 CFU/g)
143 comparable to conventional mice (Fig. 2G), demonstrating that commensal bacteria do
144 not influence *K. pintolopesii*'s intestinal colonization. The ability of *K. pintolopesii* to
145 colonize gastrointestinal tract to high levels without impacting bacterial community is in
146 contrast to other fungal species that often require microbiome manipulation to establish
147 colonization [7,8,15-17].

148 We conducted a competition assay to examine whether *K. pintolopesii* affects the
149 colonization of non-murine-specific fungi. The assay included five fungal species: *K.*
150 *pintolopesii* and four previously used to colonize mice - *S. cerevisiae, C. albicans, C.*
151 *parapsilosis*, and *C. tropicalis* [16-19] (Fig. 2H). An equal number of viable fungal cells (~2 ×
152 10^6 CFU/species) were orally administered to both conventional mice and GF mice, and
153 fecal samples were collected on days 3, 7, 14, and 22, followed by ITS sequencing.
154 Notably, *K. pintolopesii* exhibited outstanding colonization ability, out-competing the other
155 fungal species in both conventional and GF mice (Fig. 2I). In conventional mice, *K.*
156 *pintolopesii* rapidly dominated the fungal community, accounting for over 95% of the total
157 fungal population within 3 days of treatment. In GF mice, *C. albicans* was initially the

158 dominant species, with *C. tropicalis* comprising over 10% of the population until day 7.
159 However, the proportion of *K. pintolopesii* increased over time, eventually representing
160 approximately 75% of the total fungal population by days 14 and 22 (Fig. 2I). This
161 suggests that *K. pintolopesii* is capable of stable colonization in laboratory mice,
162 independent of the presence of commensal gut bacteria, and provides colonization
163 resistance against non-murine fungi.

164 **_K. pintolopesii_ colonization does not induce key anti-fungal immune responses**
165 **including expansion of neutrophils and the Th17 population**

166 Fungal colonization in the gut has been reported to trigger immune responses including
167 the expansion of neutrophils and T helper 17 cells (Th17) populations. *C. albicans*, a well-
168 studied human commensal fungus, is known to induce neutrophils and Th17 populations
169 in humans and mice [20,21]. Rewilded mice, which harbor an increased fungal population in
170 the gut, exhibited increased circulating neutrophil levels [13,14]. In addition, mucosa-
171 associated fungi induced type 17 immune responses [22]. To evaluate whether *K.*
172 *pintolopesii* also induces key anti-fungal immune responses, we measured the levels of
173 neutrophils in blood. Interestingly, *K. pintolopesii* colonization did not induce circulating
174 neutrophil levels in the peripheral blood (Fig. 3A and S2A). To mimic the systemic fungal
175 dissemination, we introduced *K. pintolopesii* intravenously in mice, comparing it with *C.*
176 *albicans* systemic infection (Fig. 3B). As expected, *C. albicans*-infected mice exhibited a
177 poor survival rate and a high fungal burden in the kidneys, along with significant
178 upregulation of *Il17* gene expression in the kidney. Intriguingly, *K. pintolopesii*-infected
179 mice did not show any pathological symptoms. All *K. pintolopesii*-infected mice survived
180 and showed low to no detectable levels of fungal burden in the kidney. Additionally, *Il17*

181 gene expression in the kidney of *K. pintolopesii*-infected mice was significantly lower,
182 approximately 14-fold lower than that observed in *C. albicans*-infected mice. (Fig. 3C –
183 E). To assess neutrophils' role in *K. pintolopesii* clearance during systemic infection, we
184 depleted neutrophils using anti-Ly-6G (1A8 clone) antibody before *K. pintolopesii* infection
185 (Fig. 3F). Despite complete neutrophil depletion, all mice survived without detectable
186 kidney fungal burden (Fig. 3G-H and S2B).

187 We assessed *K. pintolopesii*'s impact on intestinal mucosa by measuring its distance
188 from the epithelium in both small intestine and colon. The fungi were found closer to the
189 epithelium on day 5 (small intestine: ~25 μm, colon: ~42 μm, mean distance) but
190 maintained a greater distance by day 13 (small intestine: ~41 μm, colon: ~55 μm, mean
191 distance) (Fig. S3A and B). We also measured the levels of Th17, another key anti-fungal
192 immune cell in mucosal immunity, following *K. pintolopesii* colonization. Interestingly, *K.*
193 *pintolopesii* colonization did not increase Th17 cells in the small intestinal lamina propria
194 (Fig. S3C). Furthermore, the gene expression levels of *S100a8* and *S100a9* in the small
195 intestine were comparable between control and *K. pintolopesii*-colonized mice (Fig. S3D).
196 Next, to test whether type-17 immune response can antagonize *K. pintolopesii*, we
197 provided IL-17A supplementation to colonized mice (Fig. S3E). Despite the IL-17A
198 injection upregulating the expression of type 17 immunity-related genes (*Il17a*, *Reg3b*,
199 *Reg3g*, *S100a8*, and *S100a9*), the fungal burden remained unchanged compared to the
200 control mice (Fig. S3F and G) indicating that IL-17 and associated downstream effectors
201 do not limit *K. pintolopesii* burden. To assess contribution of other components of adaptive
202 immune system in *K. pintolopesii* colonization, we used Rag1 knock-out (KO) mice (Fig.
203 S4A). Neither the fungal burden nor the body weight differed between wild-type (WT) and

204 Rag1 KO mice (Fig. S4B and C). To assess the potential for systemic fungal
205 dissemination and immune activation in the absence of B and T lymphocytes, we
206 measured the number of neutrophils in the spleen. No significant differences were
207 observed in neutrophil density between the two genotypes indicating that the adaptive
208 immune arms are neither engaged nor play a significant role in limiting *K. pintolopesii*
209 burden (Fig. S4D).

210 It has been reported that intestinal colonization by *C. albicans* can protect the host
211 against systemic *C. albicans* infection [21]. To assess whether this commensal fungus
212 provides a similar cross-species protection to the host, *C. albicans* was systemically
213 introduced into *K. pintolopesii*-colonized mice (Fig. S5A). However, no differences in
214 survival rates or fungal burden in the kidneys were observed between the control and *K.*
215 *pintolopesii*-colonized mice following systemic *C. albicans* infection (Fig. S5B and C). In
216 contrast, we observed that the intestinal colonization by *C. albicans* in antibiotics-treated
217 mice protected the host from systemic candidiasis (Fig. S5D – F).

218 These results indicate that *K. pintolopesii* does not trigger classical anti-fungal defenses
219 including neutrophilia and Th17 response and the complete absence of the adaptive arm
220 of the immune system does not enhance fungal pathogenicity. When *K. pintolopesii* was
221 introduced systemically, the host was able to control the fungus via neutrophil-
222 independent mechanisms suggesting a unique host-fungal relationship that differs from
223 typical anti-fungal immune responses.

224 ***K. pintolopesii* increases the macrophage population in the small intestine**

225 Although we examined the effects of *K. pintolopesii* colonization on the host immune
226 system, we primarily focused on dominant anti-fungal immune responses, specifically

227 neutrophils and Th17 cells. However, to thoroughly investigate the impact of *K.*
228 *pintolopesii* colonization on the host's intestine in an unbiased manner, we collected ileum
229 samples 14 days post-colonization and performed bulk RNA sequencing. *K. pintolopesii*
230 colonization showed significant transcriptional changes with 602 up-regulated genes and
231 1,213 down-regulated genes compared with control mice (Fig. 4A and S6A). Notably,
232 genes associated with macrophage activation were remarkably upregulated following *K.*
233 *pintolopesii* colonization (Fig. 4B). GO terms related to macrophage activation, including
234 'regulation of macrophage activation', 'macrophage activation', and 'macrophage
235 cytokine production', were significantly enriched in the *K. pintolopesii*-colonized group
236 (Fig. 4C). We also observed that *K. pintolopesii*-colonized mice exhibited elevated
237 macrophage frequencies in the lamina propria of small intestine compared with control
238 mice (Fig. 4D and S6B).

239 To test the role of macrophages on *K. pintolopesii* colonization, we used the clodronate-
240 liposomes mediated macrophage depletion technique. Clodronate liposomes can also
241 target monocyte and monocyte-derived macrophages along with resident macrophages
242 [23,24]. Interestingly, in clodronate-treated mice, *K. pintolopesii* colonization significantly
243 increased the level of neutrophils in systemic circulation compared to non-colonized mice
244 (Fig. 4E-F and S6C). This indicates that in the absence of macrophages and monocytes,
245 *K. pintolopesii* can disseminate systemically and trigger neutrophilia. These findings
246 suggest that macrophages are a barrier to the systemic spread of *K. pintolopesii* and help
247 maintain this fungus as a commensal member within the gut.

248 ***K. pintolopesii* colonization induces type 2 immune responses in the gut and**
249 **protects the host against roundworm infection**

250 Our further analysis of the RNA-seq data revealed upregulation of tuft cell and goblet cell
251 marker genes in *K. pintolopesii*-colonized mice (Fig. 5A). To validate the RNA sequencing
252 data, we quantified the number of tuft cells and goblet cells in the small intestine. As we
253 saw in RNA sequencing data, the number of tuft cells and goblet cells was significantly
254 higher in *K. pintolopesii*-colonized mice than in control mice (Fig. 5B and C). Tuft cells are
255 a rare cell type in the intestinal epithelium, yet they play a crucial role in goblet cell
256 hyperplasia and initiating type 2 immune responses [25,26]. So, next examined *K.*
257 *pintolopesii* also modulates other type 2 associated cells. We observed significant
258 upregulation of T helper 2 (Th2) and group 2 innate lymphoid cells (ILC2s) by *K.*
259 *pintolopesii* colonization (Fig. 5D and S7A).

260 To check if this induction of type-2 immunity is not only limited to the C57BL/6 mouse
261 strain, we colonized *K. pintolopesii* in the prototypical Th2-type mice, BALB/c [27,28].
262 Colonized BALB/c mice exhibited a high fungal burden and significantly increased
263 frequencies of Th2 and ILC2 levels in the small intestine, similar to what was observed in
264 C57BL/6 mice (Fig. 5E-F and S7B). However, circulating neutrophil levels and the Th17
265 population in the small intestine were comparable to those in control mice (Fig. S7C and
266 D).

267 Next, to assess the functional relevance of this type-2 immunity, we challenged control
268 and *K. pintolopesii*-colonized mice with a murine intestinal nematode, *Heligmosomoides*
269 *polygyrus*, that is controlled by type-2 immune responses (Fig. 5G). The number of eggs
270 in the fecal samples was significantly lower in *K. pintolopesii*-colonized mice compared
271 with control mice at 21 days post-infection (Fig. 5H). This suggests that *K. pintolopesii*
272 colonization in the mouse intestine protects the host from a parasitic nematode.

273 ***K. pintolopesii* exhibits strict host specificity, with colonization of non-murine**
274 **strains causing microbiome and metabolic disruption in mice**

275 We described a mouse-originated strain of *K. pintolopesii* (Kp-M) that can stably colonize
276 the mouse intestine and remains non-virulent even when systemically exposed. Two
277 recent studies have identified other *Kazachstania* strains, from mice intestines [29,30].
278 Similarly, *Kazachstania* species have been found in pigs, primates, and humans [31-34]. The
279 presence in different hosts suggest that *Kazachstania* species are widely distributed
280 across mammals and might contribute similar symbiotic benefit to their host. However,
281 another feature of true commensal is the adaptation of the symbiont to the specific
282 environmental and physiological conditions of the natural host, borne out of long-period
283 of co-existence. There have been many examples of such host-restriction across the
284 microbiome literature [35-37]. To explore whether *K. pintolopesii* also displays such
285 colonization restriction, we isolated a different strain of *K. pintolopesii* from the gut of
286 another pet rodent, the guinea pig. The guinea pig-originated strain (Kp-GP) was isolated
287 from fecal samples based on the shape and size of colonies on the plates and was
288 identified as *K. pintolopesii* by their ITS sequences and clustered together with the Kp-M
289 strain (Fig. S8A). The genomes of Kp-M and Kp-GP were sequenced and assembled with
290 good completeness. The estimated genome sizes were 13.5 Mbp for Kp-M and 13.9 Mbp
291 for Kp-GP, with only minor differences observed in the aligned sequences between the
292 two strains (Fig. S8B - D). Average nucleotide identity (ANI) analysis revealed a 98%
293 identity between Kp-M and Kp-GP genome sequences. We obtained genome sequences
294 of additional *K. pintolopesii* strains isolated from cynomolgus macaque (KPIN-4417) and
295 mice (C89-2, ID1LA, IDNYC, QC1, W26G), as well as Kaz3, another murine commensal,

296 to conduct a comprehensive genomic analysis. The genomes of eight *K. pintolopesii*
297 strains and *K. weizmannii* showed a high level of similarity and shared a substantial
298 number of the function-known genes (Fig. S8E). We inferred the orthologs of the two *K.*
299 *pintolopesii* isolates with other fungal species and compared them using the phylogenetic
300 method, which showed that Kp-M, Kp-GP, and *K. pintolopesii* strains share more genomic
301 features with each other than with other species, such as *C. albicans* and *S. cerevisiae*
302 (Fig. S8F).

303 We first tested if Kp-GP can systemically spread through intravenous introduction.
304 Similar to Kp-M, Kp-GP showed no detectable fungal burden in the kidney and we
305 observed no differences between in body weight, circulating neutrophil levels, or kidney
306 *Il17* gene expression (Fig. S9A – E). Next, we assessed if the the Kp-GP strain can
307 establish itself in gut. But unlike the mouse-derived strain, Kp-GP showed very poor
308 colonization in the intestine of the mouse host (Fig. 6A and B). In addition, continuous Kp-
309 GP exposure in mice did not improve the colonization (Fig. S10A and B).

310 However, the colonization level of Kp-GP in the GF mice was comparable to that of Kp-
311 M (Fig. 6C), indicating that commensal bacteria provide colonization resistance to Kp-GP.
312 To investigate how commensal bacteria influence fungal colonization in a non-native host,
313 we used the Altered Schaedler Flora (ASF) model system with the defined bacterial
314 species. A further advantage of the ASF-colonized mice is, it can support stable
315 colonization of non-murine commensal fungi like *Malassezia restricta* and *C. albicans*,
316 providing an ideal system to compare colonization patterns of fungi from different host
317 origins [38,39]. We gavaged Kp-M, Kp-GP, and *C. albicans* into ASF-colonized ex-GF mice
318 and confirmed stable colonization in the intestine, although the fungal burden of Kp-GP

319 and *C. albicans*-colonized mice was significantly lower compared with Kp-M-colonized
320 mice (Fig. 6D and E). 16S rRNA gene sequencing revealed that colonization of Kp-GP
321 and *C. albicans* altered the bacterial community, whereas Kp-M did not change the ASF
322 community in the gut (Fig. 6F and G).

323 We also analyzed cecal metabolites, and similar patterns were observed (Fig. 6H).
324 Specifically, mice colonized with non-murine fungi, Kp-GP or *C. albicans*, exhibited similar
325 metabolic alterations particularly among amino acids and organic compounds (Fig. 6I).
326 To infer the effects of bacterial alteration on the cecal metabolites, we performed a co-
327 occurrence analysis and found several significant concurrent patterns between cecal
328 metabolites and intestinal bacteria. Especially two *Lactobacillus* species (ASF360 and
329 361) showed positive associations with metabolites related to 'Alanine, aspartate and
330 glutamate metabolism', 'Glycine, serine and threonine metabolism', 'Amino sugar and
331 nucleotide sugar metabolism', and 'Pantothenate and CoA biosynthesis' pathways in Kp-
332 GP or *C. albicans*-colonized mice. In contrast, *Mucispirillum schaedleri* (ASF457) and
333 *Parabacteroides* sp. (ASF519) showed negative associations with these metabolites.
334 Conversely, level of these bacteria were negatively associated with metabolites like
335 acetoin, ethylmalonate, xanthurenate, diaminopimelate, hydroxypyruvate, anserine, and
336 diacetyl (Fig. 6I). These results suggest that *K. pintolopesii* colonization in non-native host
337 alters the host's intestinal bacterial communities, potentially affecting metabolic pathways
338 and overall gut homeostasis suggesting the host's commensal bacteria act as a barrier,
339 resisting colonization by non-native *K. pintolopesii* strains.

340

341 **Discussion**

342 Naturalized, wilded, and pet store cohoused mice have emerged as valuable models for
343 studying the impact of microbes encountered outside the laboratory setting. These mice
344 provide researchers with a more accurate representation of the complex microbial
345 interactions that occur in natural environments, offering insights that conventional
346 laboratory mice cannot. Transfer of gut microbiome from wild mice to the GF mice
347 exhibited improved protection against viral infection and embryo transfer of laboratory
348 mice into wild mice showed human-like immune phenotypes [40,41]. Exposing laboratory
349 mice to wild environments, and then recapturing them, is another way to colonize the wild
350 microbiome in laboratory mice. These rewilded mice exhibit increased circulating
351 neutrophils and enhanced granulopoiesis [13,14]. Pet store mice are another valuable
352 resource for studying host-microbe interactions in mice. Although they do not live in the
353 natural environment like wild mice, they are exposed to the dirty environment in which
354 humans live. When laboratory mice are exposed to pet store mice microbiome by co-
355 housing, co-housed laboratory mice harbor various microbes such as viruses, fungi, and
356 worms, and exhibit similar immune composition to those of human adults [10,42].

357 While studies have explored interactions between mice and their complex microbiomes
358 in toto, the specific relationships between hosts and individual microbial kingdoms are
359 less explored, especially in the presence of diverse pathogenic groups. Among various
360 microbes, we focused on the role of commensal fungi in the murine gut. Fungi ubiquitously
361 exist in environments including several body sites of mammals [43]. In general, the
362 importance of commensal fungi is underestimated compared to commensal bacteria due
363 to fewer available databases and lower cell numbers compared to bacteria in the gut.

364 However, fungi can contribute unique metabolic functions as eukaryotes and even minor
365 commensal member affects host phenotypes in the gut [6,44,45]. In our study, we aimed to
366 identify murine commensal fungi that will allow us to take advantage of the robust mouse
367 model to study fungal commensalism. We successfully isolated *K. pintolopesii* from the
368 intestines of pet store mice, which constituted the dominant fungal species in the pet store
369 mice regardless of geographic location. In laboratory settings, *K. pintolopesii* was capable
370 of stable colonization without any manipulation of the gut microbiome and was not harmful
371 to the host.

372 Two recent studies also identified *Kazachstania* species from murine hosts from
373 immunodeficient and wild mice that can colonize laboratory mice gut to high numbers.
374 While the study by Kralova et al. investigates *Kazachstania heterogenica var. weizmannii*
375 isolated from an immunodeficient mouse model [29], the study by Liao et al. examines *K.*
376 *pintolopesii* isolated from free-living mice [30]. The *Kazachastania* sp. in all three studies
377 demonstrate a remarkable ability to colonize the murine gastrointestinal tract and
378 outcompete or prevent colonization by non-murine fungi including *C. albicans*,
379 showcasing their potential as powerful modulators of the gut mycobiome.

380 *K. weizmannii* exhibits a stealth colonization strategy, inducing minimal immune
381 responses under normal conditions but mitigating *C. albicans*-induced pathology [29]. In
382 contrast, *K. pintolopesii* isolated in Liao et al. and our study triggers a robust type 2
383 immune response enhancing resistance to helminth infections while exacerbating
384 gastrointestinal allergy [30]. We additionally reveal the critical role of macrophages in
385 modulating the immune response during colonization by *K. pintolopesii*, particularly in
386 preventing excessive neutrophil activation. We show that upon colonization, *K.*

387 *pintolopesii* does not trigger the typical antifungal immune responses associated with
388 other gut-colonizing fungi, such as *C. albicans*, which often leads to increased neutrophil
389 levels. Instead, the presence of *K. pintolopesii* is associated with an increase in
390 macrophage populations within the small intestine. When macrophages/monocytes are
391 depleted using clodronate-liposomes, there is a significant rise in circulating neutrophils
392 following *K. pintolopesii* colonization. Macrophages play a crucial role in maintaining
393 immune homeostasis with commensal bacteria in the gut. These tissue-resident cells are
394 strategically positioned in the intestinal lamina propria, where they act as the first line of
395 defense against potential pathogens while simultaneously promoting tolerance to
396 beneficial microbes. Unlike neutrophils, which can cause bystander damage through their
397 potent inflammatory responses, macrophages employ a more measured approach to
398 microbial interactions [46-48].

399 Our study also provides compelling evidence for species-specific host adaptation of *K.*
400 *pintolopesii*. We observed that two *K. pintolopesii* strains isolated from different hosts,
401 mice and guinea pigs, act differently in mice despite their high genomic similarity. Only
402 the mouse-derived *K. pintolopesii* strain showed stable colonization in conventional mice
403 with colonization resistance against non-murine fungal strains. However, the Kp-GP strain
404 failed to colonize the mouse gut, and the colonization level of the Kp-GP was significantly
405 lower than that of the Kp-M, even in the presence of a simple bacterial community, the
406 ASF. Moreover, the Kp-M strain did not change the bacterial composition and metabolites
407 in the gut, whereas the Kp-GP strain altered the commensal bacteria and cecal metabolic
408 profiles in the ASF mouse model. Our results demonstrate that fungal species require
409 host adaptation to establish a commensal relationship with the host in the gut. Host

410 adaptation is crucial in becoming a colonizer of the host's microbial community [49]. For
411 example, pathogenic bacteria evolve genetically to colonize new host species, allowing
412 them better adhesion ability, host-specific nutrient acquisition, and immune evasion [49].
413 Tso et al. reported that the mouse gut-adapted *C. albicans* strain by experimental
414 evolution exhibits enhanced competitive fitness in the gut [50]. Although genome
415 sequences between Kp-M and Kp-GP are highly similar, small genomic differences during
416 host adaptation may result in different colonization abilities because even a single amino
417 acid difference can provide host specificity [51]. The presence of commensal bacteria plays
418 a crucial role in supporting fungal commensalism because we observed that the Kp-GP
419 strain colonized the gut of GF mice at levels similar to those of the Kp-M strain. One
420 possible explanation is that the host-adapted fungi do not directly compete with
421 commensal bacteria for nutrients within the gut environment because the Kp-M strain did
422 not alter the bacterial community and the cecal metabolic profiles. Another possibility is
423 that the host-adapted fungi can evade the immune system, which was trained by
424 commensal bacteria. Kralova et al.'s study identifies *K. heterogenica* or *K. weizmannii* in
425 human gut and vaginal microbiome samples, suggesting potential translational
426 implications [29]. Our findings underscore the importance of considering strain-level
427 differences and unique host-specific adaptation when studying fungal commensals.

428 The Liao et al. study shows that *K. pintolopesii* triggers a type 2 immune response,
429 characterized by eosinophilia and Th2 cell polarization but only when the mucosal barrier
430 is impaired (e.g., during fiber-free diet, antibiotic treatment, or in germ-free mice) [30]. In
431 contrast, we observed that *K. pintolopesii* strain from pet store mice increases type 2
432 immune cells in the small intestine and provides cross-kingdom protection against

helminth infection even without any need of barrier impairment suggesting strain-level differences in *K. pintolopesii* mice strains between the two studies. Perhaps in the microbial environment of pet store mice that have higher burden of parasitic worms and pathogens has forced *K. pintolopesii* to induce type 2 immunity [52-54]. Cross-kingdom interactions highlight the complexity and interconnectedness of microbial communities and their host organisms. These interactions can have significant implications for understanding disease resistance, developing new therapeutic strategies, and managing ecosystems.

In conclusion, our study underscores the critical importance of strain-specific, host-exclusive commensal fungal interactions in shaping the gut mycobiome and influencing host physiology (Fig. 7). The discovery of *K. pintolopesii*'s species-level exclusivity in mice points to the intricate evolutionary adaptations enabling specific fungi to establish stable, host-specific relationships. Focusing on these naturally occurring, host-adapted fungi can provide deeper insights into co-evolutionary processes, leading to a more nuanced understanding of how commensal fungi contribute to host health, influence immune system development, and potentially protect against pathogens or modulate disease outcomes. This approach could reveal new therapeutic targets or probiotic strategies for improving gut health and managing various gastrointestinal disorders.

455 **Methods**

456 **Mice**

457 Conventional wild-type C57BL/6 mice were purchased from Taconic Biosciences and
458 Jackson laboratory or were bred in the animal facility at Brown University. BALB/c mice
459 were purchased from Jackson laboratory. Rag1 KO mice were used as an adaptive
460 immunity-deficient mouse model. Germ-free (GF) mice were wild-type C57BL/6
461 background, and they were raised and bred in flexible film isolators in a gnotobiotic facility
462 at Brown University. Pet store mice were purchased from local pet stores. Fecal pellets
463 of pet store mice in Minnesota and Texas and pet guinea pigs were freshly delivered to
464 Brown University and used for further experiments. Altered schaedler flora (ASF) mice
465 were established by colonizing GF mice with ASF. Briefly, ASF fecal pellets (Taconic
466 Biosciences) were resuspended in pre-reduced sterile PBS (50 mg/1 mL) followed by
467 filtration using the 70 μm cell strainer. 100 uL filtrates were gavaged into GF mice.
468 Experiments were performed according to the protocols approved by the Institutional
469 Animal Care and Use Committees of Brown University.

470 **Fungal isolation from the gut of pet store mice and guinea pigs**

471 Cecal contents and feces, collected from pet store mice, were suspended in sterile PBS
472 and plated on Sabouraud Dextrose (SD) agar with streptomycin (40 mg/L) followed by
473 incubation at 30 °C for 5 days. A total of 26 single colonies were randomly picked from
474 the plates and the ITS region of fungal colonies was amplified by colony PCR using the
475 Phire Green Hot Start II PCR Master Mix (Thermo Scientific) with ITS1-F/ITS4 primer pair
476 (ITS1-F: 5'-CTTGGTCATTTAGAGGAAGTAA-3', ITS4: 5'-
477 TCCTCCGCTTATTGATATGC-3') [55,56]. The amplification program consisted of 94 °C for

478 10 min, followed by 35 cycles of 94 °C for 30 sec, 52 °C for 30 sec, and 72 °C for 1 min,
479 and 72 °C for 8 min. The amplicon was sequenced by Sanger sequencing (GENEWIZ)
480 and MOLE-BLAST (Basic Local Alignment Search Tool) was performed against the ITS
481 database of NCBI to identify the isolated colonies. The exported phylogenetic tree from
482 MOLE-BLAST was visualized using the R package *ggtree*.

483 To isolate *K. pintolopesii* from pet guinea pigs, feces were suspended in sterile PBS
484 and plated on SD agar with streptomycin (40 mg/L) followed by incubation at 37 °C for 2
485 days. Nine single colonies with morphological characteristics resembling those of mouse
486 *K. pintolopesii* colonies were selected from the plates. Identifying these isolates followed
487 the same procedures as we did for pet store mice samples.

488 **Fungal culture**

489 All fungal strains were cultured in SD or yeast extract-peptone-dextrose (YPD) media.
490 The isolate, *K. pintolopesii*, was cultured at 37 °C for 1 day with shaking. This culture was
491 inoculated in fresh media and cultured for 1 day in the same condition. *S. cerevisiae*
492 BY4717 was cultured at 30 °C for 2 days with shaking. *C. albicans* SC5314, *C.*
493 *parapsilosis* ATCC22019, and *C. tropicalis* MYA-3404 were cultured overnight at 30 °C
494 with shaking. For systemic infection, *C. albicans* overnight culture was inoculated in fresh
495 media and cultured for 4 h in the same condition.

496 **Fungal infection**

497 *K. pintolopesii* were treated in drinking water (~10^6 CFU/mL) for intestinal colonization.
498 After three days, the fungal water changed to fresh regular drinking water.

499 For oral administration of various fungal species, each fungal culture was mixed with
500 the same CFU and gavaged to conventional or GF mice (~2 × 10^6 CFU/species in 200
501 μL per mouse).
502 For intestinal colonization of *C. albicans*, antibiotics water was prepared with penicillin
503 (750 U/mL), streptomycin (1 mg/mL), and 2.5% glucose. The antibiotic water was treated
504 four days before oral inoculation. *C. albicans* culture was resuspended in antibiotic water
505 (~10^6 CFU/mL) and was treated. After a day, fungal antibiotic water was changed to fresh
506 antibiotic water, and fresh antibiotic water was provided every three or four days during
507 the whole experimental period. The same antibiotics water was provided for mice in the
508 control group and the *K. pintolopesii* group.
509 For ASF mice colonization, each fungal strain was gavaged into mice after 2 weeks of
510 ASF treatment (2 × 10^6 CFU/mouse).
511 For systemic infections, *K. pintolopesii* (~10^5 CFU/200 μL) or *C. albicans* (~10^5
512 CFU/200 μL) was injected into mice via the retro-orbital venous sinus or lateral tail vein.
513 All fungal cultures were washed twice with sterile PBS and resuspended in the proper
514 solution for infection.
515 **Fungal burden measurement**
516 The fecal pellets and the contents of the intestine were resuspended in sterile PBS with
517 antibiotics (500 mg/L ampicillin, 250 mg/L streptomycin, 225 mg/L kanamycin). The other
518 tissues were homogenized in sterile PBS with antibiotics. All samples were serially diluted
519 in sterile PBS and plated on SD agar with streptomycin (40 mg/L) followed by incubation
520 at 30 °C or 37 °C for 1 or 2 days based on the optimal condition of each fungus.
521 **Immune cell isolation and flow cytometry**

522 To isolate peripheral blood lymphocytes, blood samples were collected from the
523 submandibular vein by cheek punch in heparin-containing polypropylene tubes. Red
524 blood cells were removed from blood samples by two rounds of ACK (Ammonium-
525 Chloride-Potassium) lysis buffer treatment. Lymphocytes from the spleen and the small
526 intestinal lamina propria were isolated as described in Beura et al. [57] and Grizotte-Lake
527 et al. [58].

528 Isolated cells were stained with the corresponding cocktail of fluorescently labeled
529 antibodies (CD3, CD4, CD8a, CD8b, CD11b, CD11c, CD44, CD45, CD62L, CD64,
530 CD90.2, B220, Ly6C, Ly6G, KLRG1, F4/80, ST2) and biotin-conjugated anti-mouse
531 lineage CD3e, CD5, Ly6G, CD19, CD11b, CD11c and streptavidin. Cell viability was
532 determined using Ghost Dye 780 or Fixable Viability Dye eFluor™ 450. After surface
533 staining, cells were fixed and permeabilized followed by intracellular staining with the
534 corresponding cocktail of fluorescently labeled antibodies (T-bet, Foxp3, GATA3, Rorγt,
535 IL-17). The stained samples were acquired using the Aurora flow cytometer (Cytek) and
536 were analyzed with FlowJo 10 software (BD). To visualize high-dimensional flow
537 cytometry data, 80,000 live $CD45^+$ cells per group were sampled using the DownSample
538 plugin and analyzed using the t-distributed stochastic neighbor embedding (t-SNE)
539 method in Flowjo 10 software.

540 **IL-17 injection**

541 Recombinant mouse IL-17A (BioLegend) was administered intraperitoneally to mice
542 every other day (0.5 μg/100 μL per mouse), beginning on the day of *K. pintolopesii*
543 treatment, to elevate the levels of IL-17. Control mice received intraperitoneal injections
544 of PBS (100 μL per mouse).

545 **Neutrophil and macrophage/monocyte depletion**

546 For neutrophil depletion, anti-Ly-6G antibody (1A8 clone; Biolegend) or isotype control
547 (Biolegend) was administered intraperitoneally to mice every other day (200 µg in 200 µL
548 per mouse) from the day before the *K. pintolopesii* challenge.

549 To deplete the macrophage/monocyte populations, Clodrosome (Encapsula Nano
550 Science) was administered intraperitoneally to mice every other day (200 µL per mouse)
551 from the day before *K. pintolopesii* treatment. Encapsome (Encapsula Nano Science), a
552 control liposome formulation, was administered to control *K. pintolopesii* treatment mice
553 (200 µL per mouse).

554 **Genome sequencing of fungal isolate**

555 ***DNA extraction and Sequencing.*** Fungal DNA was extracted from fungal culture as
556 described in Jiang et al [16]. Briefly, fungal cells (~10^8 CFU) were collected by centrifugation
557 at 4,000 rpm for 5 min. Cell pellets were suspended in 50 mM Tris buffer (pH 7.5)
558 supplemented with 1 mM EDTA, 0.2% b-mercaptoethanol, and 1000 units/ml of lyticase
559 (Sigma-Aldrich) followed by incubation at 37 °C for 30 min. After incubation, genomic
560 DNA was extracted using a Quick-DNA™ Fungal/Bacterial Miniprep Kit (Zymo Research).

561 The extracted DNA sample was submitted to the MiGS or the SeqCenter for library
562 construction and sequencing. For Illumina sequencing, sample libraries were prepared
563 using the Illumina DNA prep kit and IDT UDI indices and then sequenced on Illumina
564 NextSeq 2000 or NovaSeq X Plus 2 × 151 bp paired-end sequencing. Demultiplexing,
565 quality control, and adaptor trimming were performed with bcl2fastq. For Oxford
566 Nanopore Technology (ONT) sequencing, samples were prepared using the Genomic

567 DNA by Ligation kit (Oxford Nanopore) and then sequenced on Nanopore R9 flow cells.
568 Guppy was used for high-accuracy base calling.

569 ***Genome assembly and annotations.*** Adapter and low-quality sequences were trimmed
570 from Illumina reads using Trimmomatic [59]. ONT reads were trimmed and filtered using
571 Porechop [60] and Nanofilt [61]. The quality of reads before and after trimming was checked
572 using FastQC (https://www.bioinformatics.babraham.ac.uk/projects/fastqc/). The *k*-mer
573 was counted using jellyfish [62] with Illumina reads followed by visualization on
574 GenomeScope [63] to estimate genome size.

575 *De novo* assembly was performed using Flye [64] based on ONT data and the assembled
576 genome was polished with Illumina reads using medaka
577 (https://github.com/nanoporetech/medaka), Racon [65], and Pilon [66]. Assembly was
578 assessed using QUAST [67] and BUSCO [68]. Funannotate pipeline
579 (https://github.com/nextgenusfs/funannotate) was used for genome annotation.

580 ***Comparative genome analysis.*** Assembled *K. pintolopesii* genomes from mice and
581 guinea pigs were aligned using the Mauve alignment tool [69]. Anvi'o [70] was used to align
582 and visualize multiple genomes. Orthofinder [71] was used to infer orthologs between yeast
583 strains and compare their genes. All genome and protein sequences (*K. pintolopesii*
584 KPIN-4417, *K. pintolopesii* C89-2, *K. pintolopesii* ID1LA, *K. pintolopesii* IDNYC, *K.*
585 *pintolopesii* QC1, *K. pintolopesii* W26G, *K. weizmannii* Kaz3, *C. albicans* SC5314
586 ASM18296v3, and *S. cerevisiae* S288C R64) were downloaded from the NCBI database.

587 **DNA extraction for microbiome and mycobiome analysis**

588 The small intestine (ileum) and colon were flushed with sterile PBS to collect luminal
589 contents and intestinal material was obtained by centrifugation at 5,000 rpm for 10 min.

590 After the flush, the small intestine and colon were scraped and collected in sterile PBS
591 followed by centrifugation at 5,000 rpm for 10 min to get mucosal contents. Fecal samples
592 were directly collected from the rectum. Samples (~50 mg) were suspended in 50 mM
593 Tris buffer (pH 7.5) supplemented with 1 mM EDTA, 0.2% b-mercaptoethanol, and 1000
594 units/mL of lyticase (Sigma-Aldrich) followed by incubation at 37 °C for 30 min. After
595 incubation, genomic DNA was extracted from samples using a Quick-DNA Fecal/Soil
596 Microbe Microprep Kit (Zymo Research) according to the manufacturer's protocol and
597 was stored at −20°C until further processing.

598 **Bacterial load measurement**

599 Bacterial load in the feces was measured by quantitative real-time PCR (qPCR).
600 Reactions were prepared using Maxima SYBR Green/ROX qPCR Master Mix (Thermo
601 Scientific). Bacterial DNA contents in the intestine were determined by 16S rRNA gene
602 contents using the 340F/514R primer pair (340F: 5'-ACTCCTACGGGAGGCAGCAGT-3',
603 514R: 5'-ATTACCGCGGCTGCTGGC-3'). Bacterial load was expressed as a 2^{-Ct} value
604 and normalized to the weight of the starting fecal material.

605 **16S rRNA gene sequencing and bacterial community analysis**

606 The V4/V5 region of the bacterial 16S rRNA gene was amplified using the Phusion High-
607 Fidelity DNA polymerase (Thermo Scientific) with 518F/926R primer pair (518F: 5'-
608 CCAGCAGCYGCGGTAAN -3', 926R: 5'- CCGTCAATTCNTTTRAGT -3'), which were
609 conjugated with overhang adapter sequences for Illumina MiSeq. The amplification
610 program consisted of 95 °C for 3 min, followed by 35 cycles of 95 °C for 30 sec, 58 °C for
611 30 sec, and 72 °C for 30 sec, and 72 °C for 10 min. DNA libraries were constructed and

612 sequenced on Illumina MiSeq 2 × 300 bp paired-end sequencing (Rhode Island
613 Genomics and Sequencing Center).

614 The raw sequencing reads were processed using QIIME2 pipeline [72]. DADA2 [73] was
615 used to perform denoising and to construct the amplicon sequence variants (ASVs) table.
616 The pre-trained Naïve Bayes classifier on the SILVA 132 database [74] was used for
617 taxonomic assignment. Singletons and all features annotated as mitochondria or
618 chloroplast were removed from the table and the abundance of bacterial taxa was
619 expressed as a percentage of total 16S rRNA gene sequences. For alpha and beta
620 diversity, the feature table was rarefied to 10,434 reads. Shannon was used as an alpha
621 diversity index and principal coordinates analysis (PCoA) based on weighted UniFrac
622 distances was used for beta diversity. R package *qiime2R*
623 (https://github.com/jbisanz/qiime2R) was used for visualization.

624 **ITS sequencing and fungal community analysis**

625 The ITS1 region of the fungal DNA was amplified using the Phusion High-Fidelity DNA
626 polymerase (Thermo Scientific) with ITS1-F/ITS2 primer pair (ITS1-F: 5'-
627 CTTGGTCATTTAGAGGAAGTAA-3', ITS2: 5'-GCTGCGTTCTTCATCGATGC -3')[55,56],
628 which were conjugated with overhang adapter sequences for Illumina MiSeq. DNA library
629 construction and sequencing were conducted following the same procedures for 16S
630 rRNA gene sequencing.

631 The raw sequencing reads were processed using QIIME2 pipeline [72]. The reads were
632 trimmed using Q2-ITSxpress [75]. Trimmed sequence reads were denoised and sequence
633 variants were identified by DADA2 [73]. Taxonomy was assigned using a pre-trained Naïve

634 Bayes classifier on the UNITE v8.2 database [76]. Singletons were removed from the table
635 and the abundance of fungal taxa was expressed as a percentage of total sequence reads.

636 **RNA extraction from tissues**

637 Small pieces of the small intestine and the kidney were stored in RNAlater (Invitrogen).
638 Total RNA from tissues was extracted using PureLink™ RNA Mini Kit (Invitrogen) or
639 RNeasy Plus Mini Kit (Qiagen) according to the manufacturer's protocol and was stored
640 at −20°C until further processing.

641 **Quantitative PCR (qPCR)**

642 cDNA was synthesized from isolated RNA with M-MLV Reverse Transcriptase
643 (Invitrogen). qPCR reactions were prepared using Maxima SYBR Green/ROX qPCR
644 Master Mix (Thermo Scientific) with primer sets for *Il17* (F:
645 ATCAGGACGCGCAAACATGA, R: TTGGACACGCTGAGCTTTGA), *Reg3b* (F:
646 TACTGCCTTAGACCGTGCTTTCTG, R: GACATAGGGCAACTTCACCTCACA), *Reg3g*
647 (F: TTCCTGTCCTCCATGATCAAAA, R: CATCCACCTCTGTTGGGTTCA), *S100a8* (F:
648 TGTCCTCAGTTTGTGCAGAATATAAA, R: TCACCATCGCAAGGAACTCC), and
649 *S100a9* (F: GGTGGAAGCACAGTTGGCA, R: GTGTCCAGGTCCTCCATGATG) genes.
650 Gene expression was normalized to *Gapdh* (F: TGGCAAAGTGGAGATTGTTGCC, R:
651 AAGATGGTGATGGGCTTCCCG) and relative expression was calculated using the $^{\Delta\Delta}$Ct
652 method.

653 **RNA-Seq**

654 Extracted RNA samples were submitted for library construction and sequencing
655 (Novogene). The constructed libraries were sequenced on the Illumina NovaSeq X Plus
656 platform (Paired-end 150 bp). Adapter and low-quality reads were trimmed from the raw

657 sequence reads using Trimmomatic [59]. Trimmed sequence reads were aligned to the
658 mm10 mouse genome using STAR aligner [77]. DESeq2 [78] was used to identify differentially
659 expressed genes (DEGs) between groups when $P < 0.05$. R packages Complex heatmap
660 [79] and EnhancedVolcano (https://github.com/kevinblighe/EnhancedVolcano) were used
661 to draw the heatmap and volcano plot. The cell-specific gene list was obtained from
662 PanglaoDB [80] and utilized as a cell marker gene set for gene set enrichment analysis
663 (GSEA). R package clusterProfiler [81] was used to perform GSEA and gene ontology (GO)
664 enrichment analysis.

665 **Fluorescence *in situ* hybridization (FISH)**

666 The small intestine and the colon were fixed in Methacarn (Bioworld) and embedded in
667 paraffin. Tissues were sectioned at 7 μm and deparaffinized in xylene followed by
668 rehydration in 95% EtOH, 90% EtOH, and H_2O. After deparaffinization and rehydration,
669 tissue sections were hybridized into universal bacterial probes (Alexa 488-
670 GCTGCCTCCCGTAGGAGT; Alexa 488-GCAGCCACCCGTAGGTGT) and a universal
671 fungal probe (Alexa 555-CTCTGGCTTCACCCTATTC) directed against the 16S rRNA
672 gene and 28S rRNA gene, respectively. DAPI was used to stain the nucleus.

673 **Intestinal cell staining**

674 The small intestine was fixed in Methacarn (Bioworld) and embedded in paraffin. Fixed
675 tissues were sectioned at 7 μm and deparaffinized in xylene followed by rehydration in
676 100% EtOH, 95% EtOH, 70% EtOH, and H_2O.

677 For tuft cells, slides were incubated in citrate buffer (10 mM Trisodium citrate, 0.05%
678 Tween 20, pH 6.0) for 20 min at 95 °C for antigen retrieval. Slides were blocked with 1%
679 bovine serum albumin (BSA) followed by overnight incubation with rabbit anti-mouse

680 DCAMKL1 (Abcam) antibodies at 4 °C. After incubation, slides were washed and
681 incubated with goat anti-rabbit Alexa Fluor 546 (Invitrogen) secondary antibodies for 1 h
682 at room temperature. Slides were counterstained with DAPI.

683 For goblet cells, slides were incubated with Alcian blue (StatLab) for 30 min followed
684 by washing in running tap water for 2 min. Slides were counterstained with hematoxylin
685 for 2 min followed by washing in running tap water for 30 sec. The slides were 10 dips in
686 the clarifier and bluing reagent with washing in tap water, respectively. Slides were
687 dehydrated in 95% EtOH, 100% EtOH, and xylene.

688 **Scanning electron microscopy (SEM) & transmission electron microscopy (TEM)**

689 For SEM, *K. pintolopesii* cultures were washed twice with sterile PBS, and a thin layer
690 was applied to the coverslips. The coverslips were fixed in fixation buffer (2.5%
691 glutaraldehyde, 0.15 M sodium cacodylate, 2% paraformaldehyde, 2 mM calcium chloride,
692 0.1 M sucrose, pH 7.4) followed by incubation for 2 h at room temperature. For the small
693 intestine, sections of the tissue were flushed with sterile PBS and then cut into 1 cm
694 sections. They were incubated in the same fixation buffer as previously described. After
695 incubation, the coverslips were washed three times with washing buffer (2 mM calcium
696 chloride, 0.15 M sodium cacodylate, 0.1 M sucrose). After washing, samples were
697 incubated overnight in 2% osmium tetroxide, 2.5% glutaraldehyde, 0.15 M sodium
698 cacodylate, and 2% paraformaldehyde. Samples were washed with DI water three times
699 and dehydrated in an EtOH gradient as follows: 20%, 50%, 70%, 90%, 95% and then
700 100%. Each EtOH step was incubated for 20 min at room temperature and then washed
701 twice with 100% EtOH. Samples were flash dehydrated using a critical point dryer and
702 then mounted on coverslips for imaging. Thermo Apreo SEM was used for imaging.

703 For TEM, *K. pintolopesii* cultures were pelleted in the 1.5 mL Eppendorf tubes. The
704 fixation buffer was added to the tubes and incubated for 2 h at room temperature. The
705 samples were then washed three times with the washing buffer. After washing, samples
706 were incubated overnight in 2% osmium tetroxide, 2.5% glutaraldehyde, 0.15 M sodium
707 cacodylate, and 2% paraformaldehyde. Samples were washed with DI water three times,
708 followed by incubation overnight at 4 °C in saturated uranyl acetate solution. The next
709 day, samples were dehydrated in the EtOH gradient as we described in SEM preparation
710 and washed three times in 100% EtOH. Then, the samples were infiltrated with Hard
711 Spurr's resin and rocked on a rotator at room temperature. The gradient started at 25%
712 Hard Spurr's and 75% EtOH and gradually increased until 100% resin. Each step lasted
713 2 h, and the final 100% resin step was left overnight. The samples in resin were placed
714 in resin molds and then let to harden for 18-24 h at 60 °C. The pellets in resin were cut
715 with a knife into 100-200 nm sections and observed on PHILIPS 410 TEM.

716 **Metabolomics**

717 ***Metabolite extraction from serum and tissue samples.*** Frozen cecum lumen samples
718 were weighed and ground on a cryomill (Retsch). Water-soluble polar metabolites from
719 luminal contents were extracted with ice-cold 40:40:20 acetonitrile:methanol:water (25
720 mg tissue/mL extraction buffer), vortexed and incubated on ice for 10 min. Tissue samples
721 were then centrifuged at 16,000 *xg* for 30 min at 4 °C. The tissue supernatants were
722 transferred to new Eppendorf tubes and then centrifuged again at 16,000 *xg* for 30 min
723 at 4 °C to remove residual debris before liquid chromatography coupled to a mass
724 spectrometer (LC-MS) analysis. Extracts were immediately transferred to a mass
725 spectrometry vial and analyzed on an LC-MS.

726 ***Metabolite Measurements.*** Metabolite separation and analysis were performed on a
727 Vanquish Horizon UHPLC system (Thermo Fisher Scientific) coupled to the Orbitrap
728 Exploris 240 Mass Spectrometer (Thermo Fisher Scientific) as reported previously [82]. The
729 hydrophilic interaction chromatography (HILIC) LC separation was performed on an
730 XBridge BEH Amide column (2.5 µm, 2.1 mm X 150 mm, Waters, Milford, MA). Solvent
731 A is 95% water in 5% acetonitrile with 40 mM ammonium hydroxide and 20 mM acetic
732 acid. Solvent B is 80% acetonitrile in 20% water with 40 mM ammonium hydroxide and
733 20 mM acetic acid. The gradient was 0 min, 100% B; 3 min, 100% B; 3.2 min, 90% B; 6.2
734 min, 90% B; 6.5 min, 80% B; 10.5 min, 80% B; 10.7 min, 70% B; 13.5 min, 70% B; 13.7
735 min, 45% B; 16 min, 45% B; 16.5 min, 100% B; and 22 min, 100% B. The flow rate was
736 300 µL/min. The column temperature was set to 30 °C. The autosampler temperature
737 was set to 4 °C, and the injection volume was 5 µL. MS scans were obtained in both
738 negative and positive ion modes with a resolution of 120,000 at m/z 200, in addition to an
739 automatic gain control target of 3 x 10^6 and m/z scan range of 72 to 1000.

740 Raw LC/MS data were converted to mzML format using the command line "msconvert"
741 utility [83]. Data were analyzed via MAVEN software and the annotations of the metabolites
742 were confirmed using our in-house library generated using the Mass Spectrometry
743 Metabolite Library (Millipore Sigma, supplied by IROA Technologies). MetaboAnalyst 6.0
744 [84] was used for statistical analyses and visualization.

745 ***Heligmosomoides polygyrus* infection**

746 *H. polygyrus* L3 larvae were orally gavaged to mice (200 L3 larvae per mouse). After
747 infection, fecal samples were collected every week. Fecal samples were resuspended in
748 water and mixed with the same volume of super-saturated salt solution. The resuspended

749 fecal solution was immediately loaded on a McMaster counting chamber (Eggzamin) and
750 eggs were counted under the microscope. The counted eggs were normalized by fecal
751 weight.

752 **Statistical analysis**

753 All statistical analysis and plotting were performed on R (https://www.R-project.org) and
754 Prism (GraphPad). The normality of data was assessed by the Shapiro-Wilk test. If data
755 followed normal distribution, parametric tests (unpaired two-tailed t-test for two groups,
756 One-way ANOVA with Tukey's multiple comparisons test for more than two groups) were
757 performed. If data did not follow normal distribution, non-parametric tests (Mann-Whitney
758 test for two groups, Kruskal-Wallis test with Dunn's multiple comparisons test for more
759 than two groups) were performed to find significant differences between groups. For the
760 survival curve, the log-rank (Mantel-Cox) test was used to find significant differences
761 between groups. A two-way ANOVA test was used to find significant differences in body
762 weight changes at each time point between the two groups. *$p < 0.05$, **$p < 0.01$, ***$p <$
763 0.001, ****$p<0.0001$.

764

765

766

767

768

769

770

771

Data availability

Raw sequence reads from 16S and ITS sequencing have been deposited in the NCBI Sequence Read Archive (SRA) under accession number PRJNA1183864. The draft genome sequences of *K. pintolopesii* isolates have been deposited in the NCBI GenBank under accession numbers JARWBK000000000 and JBJCYV000000000. Bulk RNA-seq data has been deposited in the NCBI GEO database under accession number GSE281418. This paper does not report the original code.

Acknowledgments

Schematics were created with BioRender.com. We thank Dr. Richard Bennett (Brown University) for providing *S. cerevisiae* BY4717, *C. albicans* SC5314, *C. parapsilosis* ATCC22019, and *C. tropicalis* MYA-3404 strains. GH was supported by an American Association of Immunologists Careers in Immunology Fellowship. NNJ is supported by the Damon Runyon Cancer Research Foundation (DRG-2427-21) and NIAID 1K22AI177360-01. SV is supported by R01DK113265, P20GM109035 (pilot project) and Brown University Seed grant. LKB is supported by Searle Scholar Foundation and this work is also supported by Brown University Seed grant. The Thermo Apreo VS SEM was purchased with a high-end instrumentation grant from the Office of the Director at the National Institutes of Health (S10OD023461).

Author contributions

Conceptualization: SV, LKB, GH; Methodology: SV, LKB, GH, RY, MHH, NNJ, KC; Investigation: SV, LKB, GH, RY, MHH, AB, KB, JP, OL, DMM, KC; Resources: SV, LKB, NNJ; Funding acquisition: SV, LKB; Supervision: SV, LKB; Writing – original draft: SV, LKB, GH; Writing – review & editing: SV, LKB, GH, KC

Competing interests

The authors declare no competing interests.

802 **References**

803 1 Koropatnick, T. A. *et al.* Microbial factor-mediated development in a host-
804 bacterial mutualism. *Science* **306**, 1186-1188 (2004).
805 https://doi.org:10.1126/science.1102218
806 2 Pais, R., Lohs, C., Wu, Y., Wang, J. & Aksoy, S. The obligate mutualist
807 Wigglesworthia glossinidia influences reproduction, digestion, and immunity
808 processes of its host, the tsetse fly. *Appl Environ Microbiol* **74**, 5965-5974 (2008).
809 https://doi.org:10.1128/AEM.00741-08
810 3 Chung, H. *et al.* Gut immune maturation depends on colonization with a host-
811 specific microbiota. *Cell* **149**, 1578-1593 (2012).
812 https://doi.org:10.1016/j.cell.2012.04.037
813 4 Tannock, G. W., Miller, J. R. & Savage, D. C. Host specificity of filamentous,
814 segmented microorganisms adherent to the small bowel epithelium in mice and
815 rats. *Appl Environ Microbiol* **47**, 441-442 (1984).
816 https://doi.org:10.1128/aem.47.2.441-442.1984
817 5 Gaboriau-Routhiau, V. *et al.* The key role of segmented filamentous bacteria in
818 the coordinated maturation of gut helper T cell responses. *Immunity* **31**, 677-689
819 (2009). https://doi.org:10.1016/j.immuni.2009.08.020
820 6 Ivanov, II *et al.* Induction of intestinal Th17 cells by segmented filamentous
821 bacteria. *Cell* **139**, 485-498 (2009). https://doi.org:10.1016/j.cell.2009.09.033
822 7 Koh, A. Y. Murine models of Candida gastrointestinal colonization and
823 dissemination. *Eukaryot Cell* **12**, 1416-1422 (2013).
824 https://doi.org:10.1128/EC.00196-13

825 8 Koh, A. Y., Kohler, J. R., Coggshall, K. T., Van Rooijen, N. & Pier, G. B. Mucosal
826 damage and neutropenia are required for Candida albicans dissemination. *PLoS*
827 *Pathog* **4**, e35 (2008). https://doi.org:10.1371/journal.ppat.0040035
828 9 Kumamoto, C. A. Inflammation and gastrointestinal Candida colonization. *Curr*
829 *Opin Microbiol* **14**, 386-391 (2011). https://doi.org:10.1016/j.mib.2011.07.015
830 10 Beura, L. K. *et al.* Normalizing the environment recapitulates adult human
831 immune traits in laboratory mice. *Nature* **532**, 512-516 (2016).
832 https://doi.org:10.1038/nature17655
833 11 Abolins, S. *et al.* The comparative immunology of wild and laboratory mice, Mus
834 musculus domesticus. *Nat Commun* **8**, 14811 (2017).
835 https://doi.org:10.1038/ncomms14811
836 12 Ma, J. *et al.* Laboratory mice with a wild microbiota generate strong allergic
837 immune responses. *Sci Immunol* **8**, eadf7702 (2023).
838 https://doi.org:10.1126/sciimmunol.adf7702
839 13 Yeung, F. *et al.* Altered Immunity of Laboratory Mice in the Natural Environment
840 Is Associated with Fungal Colonization. *Cell Host Microbe* **27**, 809-822 e806
841 (2020). https://doi.org:10.1016/j.chom.2020.02.015
842 14 Chen, Y. H. *et al.* Rewilding of laboratory mice enhances granulopoiesis and
843 immunity through intestinal fungal colonization. *Sci Immunol* **8**, eadd6910 (2023).
844 https://doi.org:10.1126/sciimmunol.add6910
845 15 Hedin, K. A. *et al.* Effects of broad-spectrum antibiotics on the colonisation of
846 probiotic yeast Saccharomyces boulardii in the murine gastrointestinal tract. *Sci*
847 *Rep* **12**, 8862 (2022). https://doi.org:10.1038/s41598-022-12806-0

848 16 Jiang, T. T. *et al.* Commensal Fungi Recapitulate the Protective Benefits of
849 Intestinal Bacteria. *Cell Host Microbe* **22**, 809-816 e804 (2017).
850 https://doi.org:10.1016/j.chom.2017.10.013
851 17 Mellado, E. *et al.* Sustained gastrointestinal colonization and systemic
852 dissemination by Candida albicans, Candida tropicalis and Candida parapsilosis
853 in adult mice. *Diagn Microbiol Infect Dis* **38**, 21-28 (2000).
854 https://doi.org:10.1016/s0732-8893(00)00165-6
855 18 Ost, K. S. & Round, J. L. Commensal fungi in intestinal health and disease. *Nat*
856 *Rev Gastroenterol Hepatol* **20**, 723-734 (2023). https://doi.org:10.1038/s41575-
857 023-00816-w
858 19 Roberts, K. *et al.* Candida tropicalis Affects Candida albicans Virulence by
859 Limiting Its Capacity to Adhere to the Host Intestinal Surface, Leading to
860 Decreased Susceptibility to Colitis in Mice. *J Fungi (Basel)* **10** (2024).
861 https://doi.org:10.3390/jof10040245
862 20 Bacher, P. *et al.* Human Anti-fungal Th17 Immunity and Pathology Rely on
863 Cross-Reactivity against Candida albicans. *Cell* **176**, 1340-1355 e1315 (2019).
864 https://doi.org:10.1016/j.cell.2019.01.041
865 21 Shao, T. Y. *et al.* Commensal Candida albicans Positively Calibrates Systemic
866 Th17 Immunological Responses. *Cell Host Microbe* **25**, 404-417 e406 (2019).
867 https://doi.org:10.1016/j.chom.2019.02.004
868 22 Leonardi, I. *et al.* Mucosal fungi promote gut barrier function and social behavior
869 via Type 17 immunity. *Cell* **185**, 831-846 e814 (2022).
870 https://doi.org:10.1016/j.cell.2022.01.017

871 23 Huang, L., Nazarova, E. V., Tan, S., Liu, Y. & Russell, D. G. Growth of
872 Mycobacterium tuberculosis in vivo segregates with host macrophage
873 metabolism and ontogeny. *J Exp Med* **215**, 1135-1152 (2018).
874 https://doi.org:10.1084/jem.20172020
875 24 Culemann, S. *et al.* Stunning of neutrophils accounts for the anti-inflammatory
876 effects of clodronate liposomes. *J Exp Med* **220** (2023).
877 https://doi.org:10.1084/jem.20220525
878 25 Gerbe, F. *et al.* Intestinal epithelial tuft cells initiate type 2 mucosal immunity to
879 helminth parasites. *Nature* **529**, 226-230 (2016).
880 https://doi.org:10.1038/nature16527
881 26 Howitt, M. R. *et al.* Tuft cells, taste-chemosensory cells, orchestrate parasite type
882 2 immunity in the gut. *Science* **351**, 1329-1333 (2016).
883 https://doi.org:10.1126/science.aaf1648
884 27 Sasaki, S., Ishida, Y., Nishio, N., Ito, S. & Isobe, K. Thymic involution correlates
885 with severe ulcerative colitis induced by oral administration of dextran sulphate
886 sodium in C57BL/6 mice but not in BALB/c mice. *Inflammation* **31**, 319-328
887 (2008). https://doi.org:10.1007/s10753-008-9081-3
888 28 Tsuchiya, T. *et al.* Role of gamma delta T cells in the inflammatory response of
889 experimental colitis mice. *J Immunol* **171**, 5507-5513 (2003).
890 https://doi.org:10.4049/jimmunol.171.10.5507
891 29 Sekeresova Kralova, J. *et al.* Competitive fungal commensalism mitigates
892 candidiasis pathology. *J Exp Med* **221** (2024).
893 https://doi.org:10.1084/jem.20231686

894 30 Liao, Y. *et al.* Fungal symbiont transmitted by free-living mice promotes type 2
895 immunity. *Nature* (2024). https://doi.org:10.1038/s41586-024-08213-2
896 31 Hu, J. *et al.* Core-predominant gut fungus Kazachstania slooffiae promotes
897 intestinal epithelial glycolysis via lysine desuccinylation in pigs. *Microbiome* **11**,
898 31 (2023). https://doi.org:10.1186/s40168-023-01468-3
899 32 Zhang, H. *et al.* Immune activation of characteristic gut mycobiota Kazachstania
900 pintolopesii on IL-23/IL-17R signaling in ankylosing spondylitis. *Front Cell Infect*
901 *Microbiol* **12**, 1035366 (2022). https://doi.org:10.3389/fcimb.2022.1035366
902 33 Gallotti, A. C. *et al.* Kazachstania slooffiae, an emerging pathogen to watch for in
903 humans? *Med Mycol Case Rep* **42**, 100604 (2023).
904 https://doi.org:10.1016/j.mmcr.2023.08.007
905 34 Brunet, K. *et al.* Invasive Candida bovina Infection, France. *Emerg Infect Dis* **26**,
906 626-627 (2020). https://doi.org:10.3201/eid2603.191371
907 35 Flannigan, K. L. & Denning, T. L. Segmented filamentous bacteria-induced
908 immune responses: a balancing act between host protection and autoimmunity.
909 *Immunology* **154**, 537-546 (2018). https://doi.org:10.1111/imm.12950
910 36 Baumler, A. & Fang, F. C. Host specificity of bacterial pathogens. *Cold Spring*
911 *Harb Perspect Med* **3**, a010041 (2013).
912 https://doi.org:10.1101/cshperspect.a010041
913 37 Gutierrez-Garcia, K. *et al.* A conserved bacterial genetic basis for commensal-
914 host specificity. *Science* **386**, 1117-1122 (2024).
915 https://doi.org:10.1126/science.adp7748

916 38 Limon, J. J. *et al.* Malassezia Is Associated with Crohn's Disease and
917 Exacerbates Colitis in Mouse Models. *Cell Host Microbe* **25**, 377-388 e376
918 (2019). https://doi.org:10.1016/j.chom.2019.01.007
919 39 Li, X. V. *et al.* Immune regulation by fungal strain diversity in inflammatory bowel
920 disease. *Nature* **603**, 672-678 (2022). https://doi.org:10.1038/s41586-022-04502-
921 w
922 40 Rosshart, S. P. *et al.* Wild Mouse Gut Microbiota Promotes Host Fitness and
923 Improves Disease Resistance. *Cell* **171**, 1015-1028 e1013 (2017).
924 https://doi.org:10.1016/j.cell.2017.09.016
925 41 Rosshart, S. P. *et al.* Laboratory mice born to wild mice have natural microbiota
926 and model human immune responses. *Science* **365** (2019).
927 https://doi.org:10.1126/science.aaw4361
928 42 Huggins, M. A. *et al.* Microbial Exposure Enhances Immunity to Pathogens
929 Recognized by TLR2 but Increases Susceptibility to Cytokine Storm through
930 TLR4 Sensitization. *Cell Rep* **28**, 1729-1743 e1725 (2019).
931 https://doi.org:10.1016/j.celrep.2019.07.028
932 43 Netea, M. G., Joosten, L. A., van der Meer, J. W., Kullberg, B. J. & van de
933 Veerdonk, F. L. Immune defence against Candida fungal infections. *Nat Rev*
934 *Immunol* **15**, 630-642 (2015). https://doi.org:10.1038/nri3897
935 44 Underhill, D. M. & Iliev, I. D. The mycobiota: interactions between commensal
936 fungi and the host immune system. *Nat Rev Immunol* **14**, 405-416 (2014).
937 https://doi.org:10.1038/nri3684

938 45 Han, G., Luong, H. & Vaishnava, S. Low abundance members of the gut
939 microbiome exhibit high immunogenicity. *Gut Microbes* **14**, 2104086 (2022).
940 https://doi.org:10.1080/19490976.2022.2104086
941 46 Muller, P. A., Matheis, F. & Mucida, D. Gut macrophages: key players in
942 intestinal immunity and tissue physiology. *Curr Opin Immunol* **62**, 54-61 (2020).
943 https://doi.org:10.1016/j.coi.2019.11.011
944 47 Mowat, A. M. & Bain, C. C. Mucosal macrophages in intestinal homeostasis and
945 inflammation. *J Innate Immun* **3**, 550-564 (2011).
946 https://doi.org:10.1159/000329099
947 48 Wang, S., Ye, Q. H., Zeng, X. F. & Qiao, S. Y. Functions of Macrophages in the
948 Maintenance of Intestinal Homeostasis. *J Immunol Res* **2019** (2019).
949 https://doi.org:Artn 1512969
950 10.1155/2019/1512969
951 49 Barber, M. F. & Fitzgerald, J. R. Mechanisms of host adaptation by bacterial
952 pathogens. *Fems Microbiol Rev* **48** (2024).
953 https://doi.org:10.1093/femsre/fuae019
954 50 Tso, G. H. W. *et al.* Experimental evolution of a fungal pathogen into a gut
955 symbiont. *Science* **362**, 589-595 (2018). https://doi.org:10.1126/science.aat0537
956 51 Lecuit, M. *et al.* A single amino acid in E-cadherin responsible for host specificity
957 towards the human pathogen Listeria monocytogenes. *EMBO J* **18**, 3956-3963
958 (1999). https://doi.org:10.1093/emboj/18.14.3956

959 52 Roble, G. S., Gillespie, V. & Lipman, N. S. Infectious disease survey of Mus
960 musculus from pet stores in New York City. *J Am Assoc Lab Anim Sci* **51**, 37-41
961 (2012).
962 53 Parker, S. E., Malone, S., Bunte, R. M. & Smith, A. L. Infectious diseases in wild
963 mice (Mus musculus) collected on and around the University of Pennsylvania
964 (Philadelphia) Campus. *Comp Med* **59**, 424-430 (2009).
965 54 Dammann, P. *et al.* Infectious microorganisms in mice (Mus musculus)
966 purchased from commercial pet shops in Germany. *Lab Anim* **45**, 271-275
967 (2011). https://doi.org:10.1258/la.2011.010183
968 55 Gardes, M. & Bruns, T. D. ITS primers with enhanced specificity for
969 basidiomycetes--application to the identification of mycorrhizae and rusts. *Mol*
970 *Ecol* **2**, 113-118 (1993). https://doi.org:10.1111/j.1365-294x.1993.tb00005.x
971 56 White, T. J., Bruns, T., Lee, S. & Taylor, J. in *PCR Protocols: A Guide to*
972 *Methods and Applications* (eds M. A. Innis, D. H. Gelfand, J. J. Sninsky, & T. J.
973 White) 315-322 (Academic Press, 1990).
974 57 Beura, L. K. *et al.* Lymphocytic choriomeningitis virus persistence promotes
975 effector-like memory differentiation and enhances mucosal T cell distribution. *J*
976 *Leukoc Biol* **97**, 217-225 (2015). https://doi.org:10.1189/jlb.1HI0314-154R
977 58 Grizotte-Lake, M. *et al.* Commensals Suppress Intestinal Epithelial Cell Retinoic
978 Acid Synthesis to Regulate Interleukin-22 Activity and Prevent Microbial
979 Dysbiosis. *Immunity* **49**, 1103-1115 e1106 (2018).
980 https://doi.org:10.1016/j.immuni.2018.11.018

981 59 Bolger, A. M., Lohse, M. & Usadel, B. Trimmomatic: a flexible trimmer for Illumina
982 sequence data. *Bioinformatics* **30**, 2114-2120 (2014).
983 https://doi.org:10.1093/bioinformatics/btu170
984 60 Wick, R. R., Judd, L. M., Gorrie, C. L. & Holt, K. E. Completing bacterial genome
985 assemblies with multiplex MinION sequencing. *Microb Genom* **3**, e000132
986 (2017). https://doi.org:10.1099/mgen.0.000132
987 61 De Coster, W., D'Hert, S., Schultz, D. T., Cruts, M. & Van Broeckhoven, C.
988 NanoPack: visualizing and processing long-read sequencing data. *Bioinformatics*
989 **34**, 2666-2669 (2018). https://doi.org:10.1093/bioinformatics/bty149
990 62 Marcais, G. & Kingsford, C. A fast, lock-free approach for efficient parallel
991 counting of occurrences of k-mers. *Bioinformatics* **27**, 764-770 (2011).
992 https://doi.org:10.1093/bioinformatics/btr011
993 63 Vurture, G. W. *et al.* GenomeScope: fast reference-free genome profiling from
994 short reads. *Bioinformatics* **33**, 2202-2204 (2017).
995 https://doi.org:10.1093/bioinformatics/btx153
996 64 Kolmogorov, M., Yuan, J., Lin, Y. & Pevzner, P. A. Assembly of long, error-prone
997 reads using repeat graphs. *Nat Biotechnol* **37**, 540-546 (2019).
998 https://doi.org:10.1038/s41587-019-0072-8
999 65 Vaser, R., Sovic, I., Nagarajan, N. & Sikic, M. Fast and accurate de novo
1000 genome assembly from long uncorrected reads. *Genome Res* **27**, 737-746
1001 (2017). https://doi.org:10.1101/gr.214270.116

1002 66 Walker, B. J. *et al.* Pilon: an integrated tool for comprehensive microbial variant
1003 detection and genome assembly improvement. *PLoS One* **9**, e112963 (2014).
1004 https://doi.org:10.1371/journal.pone.0112963
1005 67 Gurevich, A., Saveliev, V., Vyahhi, N. & Tesler, G. QUAST: quality assessment
1006 tool for genome assemblies. *Bioinformatics* **29**, 1072-1075 (2013).
1007 https://doi.org:10.1093/bioinformatics/btt086
1008 68 Manni, M., Berkeley, M. R., Seppey, M., Simao, F. A. & Zdobnov, E. M. BUSCO
1009 Update: Novel and Streamlined Workflows along with Broader and Deeper
1010 Phylogenetic Coverage for Scoring of Eukaryotic, Prokaryotic, and Viral
1011 Genomes. *Mol Biol Evol* **38**, 4647-4654 (2021).
1012 https://doi.org:10.1093/molbev/msab199
1013 69 Darling, A. C., Mau, B., Blattner, F. R. & Perna, N. T. Mauve: multiple alignment
1014 of conserved genomic sequence with rearrangements. *Genome Res* **14**, 1394-
1015 1403 (2004). https://doi.org:10.1101/gr.2289704
1016 70 Eren, A. M. *et al.* Community-led, integrated, reproducible multi-omics with
1017 anvi'o. *Nat Microbiol* **6**, 3-6 (2021). https://doi.org:10.1038/s41564-020-00834-3
1018 71 Emms, D. M. & Kelly, S. OrthoFinder: phylogenetic orthology inference for
1019 comparative genomics. *Genome Biol* **20**, 238 (2019).
1020 https://doi.org:10.1186/s13059-019-1832-y
1021 72 Bolyen, E. *et al.* Reproducible, interactive, scalable and extensible microbiome
1022 data science using QIIME 2. *Nat Biotechnol* **37**, 852-857 (2019).
1023 https://doi.org:10.1038/s41587-019-0209-9

1024 73 Callahan, B. J. *et al.* DADA2: High-resolution sample inference from Illumina
1025 amplicon data. *Nat Methods* **13**, 581-583 (2016).
1026 https://doi.org:10.1038/nmeth.3869
1027 74 Yilmaz, P. *et al.* The SILVA and "All-species Living Tree Project (LTP)"
1028 taxonomic frameworks. *Nucleic Acids Res* **42**, D643-648 (2014).
1029 https://doi.org:10.1093/nar/gkt1209
1030 75 Rivers, A. R., Weber, K. C., Gardner, T. G., Liu, S. & Armstrong, S. D. ITSxpress:
1031 Software to rapidly trim internally transcribed spacer sequences with quality
1032 scores for marker gene analysis. *F1000Res* **7**, 1418 (2018).
1033 https://doi.org:10.12688/f1000research.15704.1
1034 76 Nilsson, R. H. *et al.* The UNITE database for molecular identification of fungi:
1035 handling dark taxa and parallel taxonomic classifications. *Nucleic Acids Res* **47**,
1036 D259-D264 (2019). https://doi.org:10.1093/nar/gky1022
1037 77 Dobin, A. *et al.* STAR: ultrafast universal RNA-seq aligner. *Bioinformatics* **29**, 15-
1038 21 (2013). https://doi.org:10.1093/bioinformatics/bts635
1039 78 Love, M. I., Huber, W. & Anders, S. Moderated estimation of fold change and
1040 dispersion for RNA-seq data with DESeq2. *Genome Biol* **15**, 550 (2014).
1041 https://doi.org:10.1186/s13059-014-0550-8
1042 79 Gu, Z. Complex heatmap visualization. *Imeta* **1**, e43 (2022).
1043 https://doi.org:10.1002/imt2.43
1044 80 Franzen, O., Gan, L. M. & Bjorkegren, J. L. M. PanglaoDB: a web server for
1045 exploration of mouse and human single-cell RNA sequencing data. *Database*
1046 *(Oxford)* **2019** (2019). https://doi.org:10.1093/database/baz046

1047 81 Xu, S. *et al.* Using clusterProfiler to characterize multiomics data. *Nat Protoc* **19**,
1048 3292-3320 (2024). https://doi.org:10.1038/s41596-024-01020-z
1049 82 Wang, L. *et al.* Peak Annotation and Verification Engine for Untargeted LC-MS
1050 Metabolomics. *Anal Chem* **91**, 1838-1846 (2019).
1051 https://doi.org:10.1021/acs.analchem.8b03132
1052 83 Adusumilli, R. & Mallick, P. Data Conversion with ProteoWizard msConvert.
1053 *Methods Mol Biol* **1550**, 339-368 (2017). https://doi.org:10.1007/978-1-4939-
1054 6747-6_23
1055 84 Pang, Z. *et al.* MetaboAnalyst 6.0: towards a unified platform for metabolomics
1056 data processing, analysis and interpretation. *Nucleic Acids Res* **52**, W398-W406
1057 (2024). https://doi.org:10.1093/nar/gkae253

1058

1059

1060 **Figures**

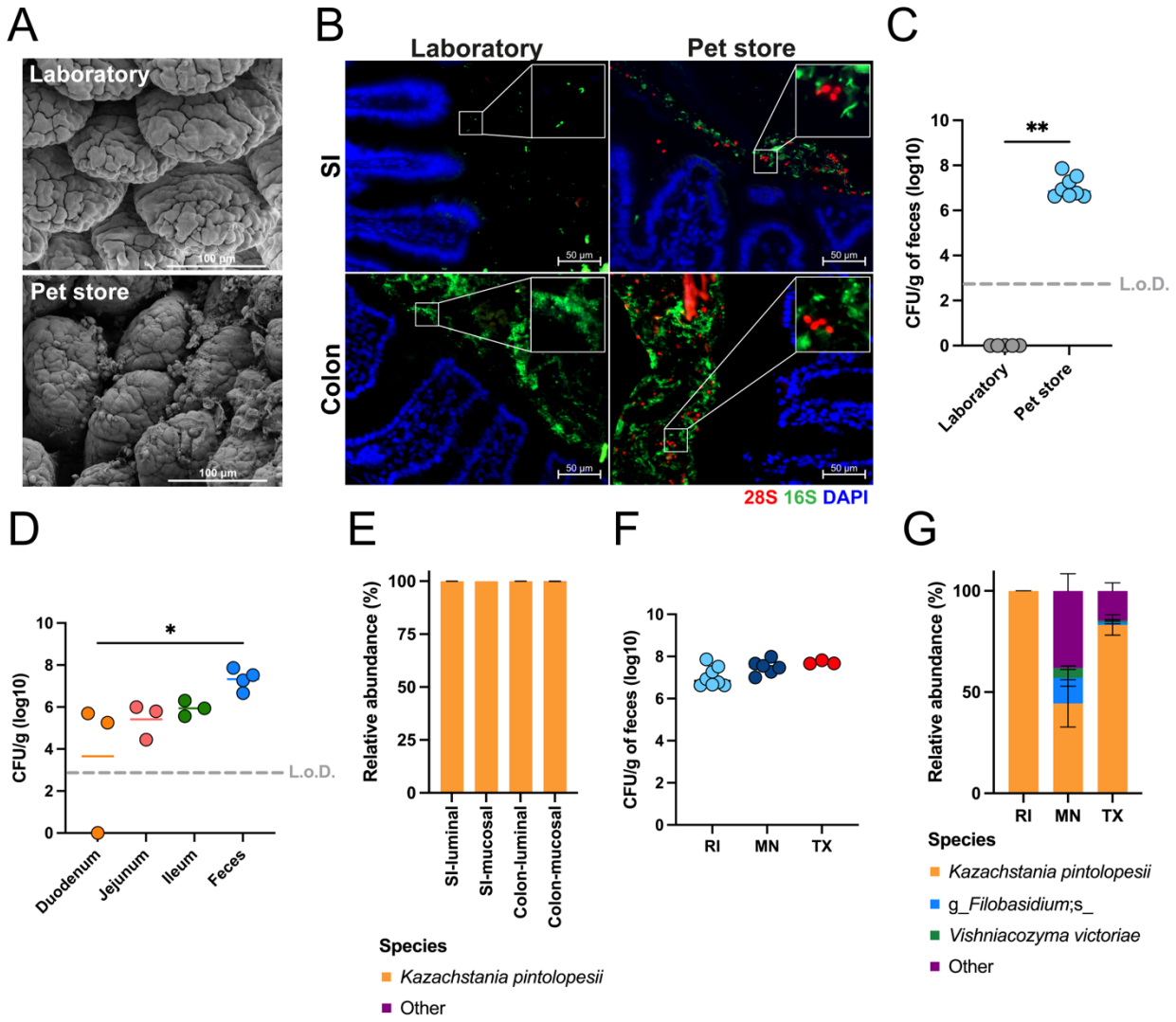

1061

1062 **Fig. 1. *K. pintolopesii* is the dominant fungus in the gut of pet store mice.** (A)
1063 Representative scanning electron microscopy (SEM) image of the small intestine of
1064 laboratory mice and pet store mice. (B) Representative fluorescence *in situ* hybridization
1065 (FISH) images of fungal colonization in the small intestine and the colon of laboratory
1066 mice and pet store mice. Tissues were stained with DAPI (nuclei; blue), EUB338 probe
1067 (bacteria; green), and 28S probe (fungi; red). (C) Fungal burden in the feces of laboratory
1068 mice (n = 5) and pet store mice (n = 8). (D) Fungal burden in the intestinal tract in the pet

1069 store mice (*n* = 3 for tissues and *n* = 4 for feces). (E) Bar plot of relative abundance of
1070 fungal species from ITS-marker gene sequencing at different sections of the intestine –
1071 luminal and mucosal part of the small intestine and the colon (*n* = 4 for SI-mucosal and *n*
1072 = 5 for other samples). Fungal burden (F) (RI, *n* = 8; MN, *n* = 6; TX, *n* =3) and bar plot of
1073 relative abundance of fungal species (G) in the feces of pet store mice (RI, *n* = 5; MN, *n*
1074 = 6; TX, *n* =8) in Rhode Island (RI), Minnesota (MI), and Texas (TX) in the USA. Bars
1075 indicate mean ± SEM. Significances were determined by the Kruskal-Wallis test with
1076 Dunn's multiple comparisons test or the Mann-Whitney test. *$p < 0.05$ and **$p < 0.01$.
1077 L.o.D., limit of detection.

1078

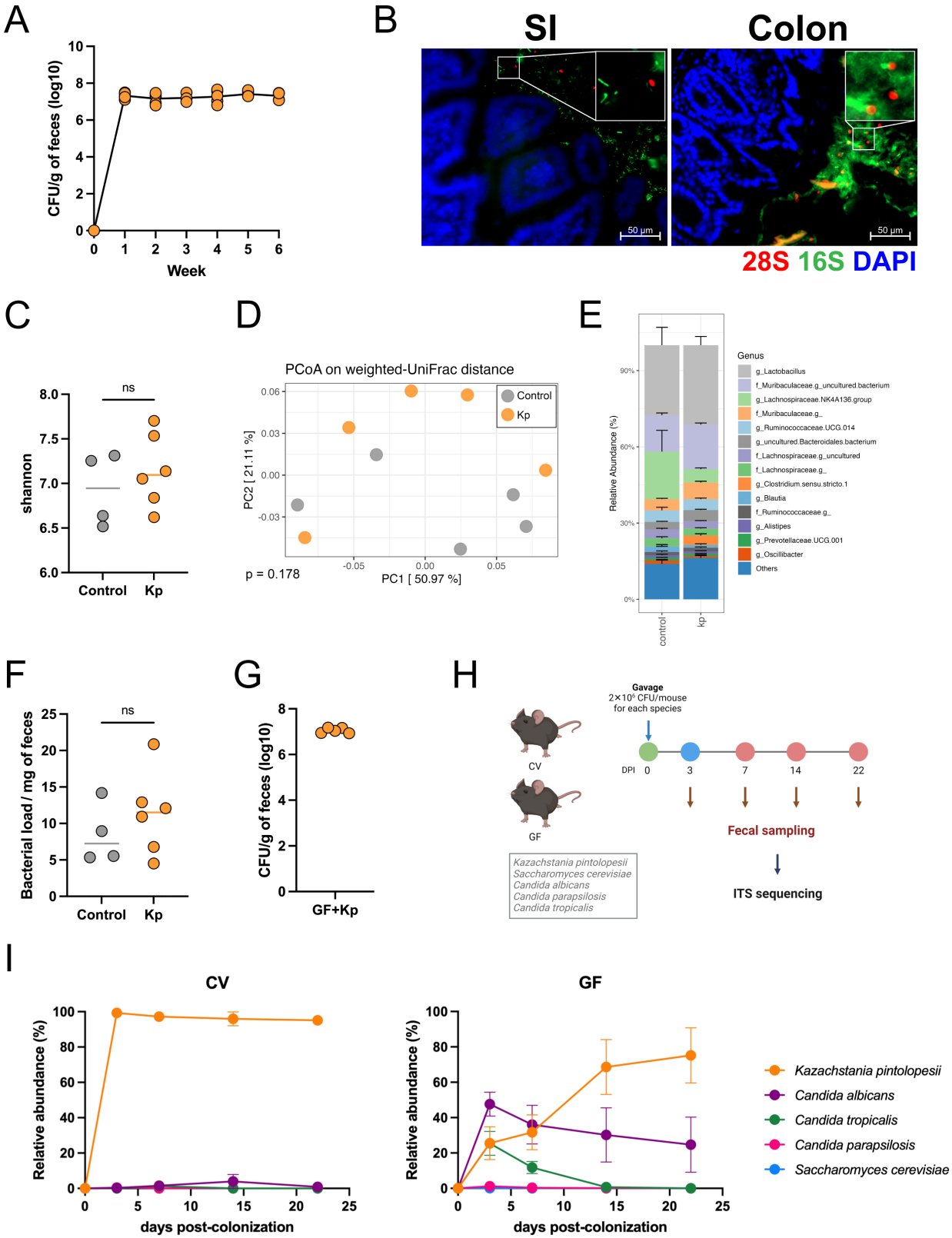
A
CFU/g of feces (log10)
Week
B
SI
Colon
50 µm
28S 16S DAPI
C
ns
shannon
Control
Kp
D
PCoA on weighted-UniFrac distance
Control
Kp
PC2 [21.11 %]
PC1 [50.97 %]
p = 0.178
E
Relative Abundance (%)
control
kp
Genus
g_Lactobacillus
f_Muribaculaceae.g_uncultured.bacterium
g_Lachnospiraceae.NK4A136.group
f_Muribaculaceae.g_
g_Ruminococcaceae.UCG.014
g_uncultured.Bacteroidales.bacterium
f_Lachnospiraceae.g_uncultured
f_Lachnospiraceae.g_
g_Clostridium.sensu.stricto.1
g_Blautia
f_Ruminococcaceae.g_
g_Alistipes
g_Prevotellaceae.UCG.001
g_Oscillibacter
Others
F
ns
Bacterial load / mg of feces
Control
Kp
G
CFU/g of feces (log10)
GF+Kp
H
CV
GF
Gavage
2×10⁶ CFU/mouse
for each species
DPI 0 3 7 14 22
Fecal sampling
ITS sequencing
Kazachstania pintolopesii
Saccharomyces cerevisiae
Candida albicans
Candida parapsilosis
Candida tropicalis
I
CV
GF
Relative abundance (%)
days post-colonization
Kazachstania pintolopesii
Candida albicans
Candida tropicalis
Candida parapsilosis
Saccharomyces cerevisiae

1079

1080 **Fig. 2. *K. pintolopesii* stably colonizes laboratory mice irrespective of gut bacteria**
1081 **and provides colonization resistance against non-murine fungi.** (A) Fungal burden
1082 in the feces of mice after *K. pintolopesii* treatment (n = 5). (B) Representative images of
1083 *K. pintolopesii* colonization at 13 days post-colonization in the small intestine and colon.
1084 Tissues were stained with DAPI (nuclei; blue), EUB338 probe (bacteria; green), and 28S
1085 probe (fungi; red). (C-E) 16S rRNA gene sequencing was performed to explore fecal
1086 bacterial communities (Control, n = 4; Kp, n = 6). (C) Alpha diversity (Shannon) at 14 days
1087 post-colonization in the feces of control and *K. pintolopesii*-colonized mice. (D) PCoA
1088 plots based on the weighted-UniFrac distances at 14 days post-colonization in the feces.
1089 Significances were determined by PERMANOVA. (E) Bar plot of relative abundance of
1090 the bacterial genus from 16S rRNA gene sequencing of the feces. (F) Bacterial load in
1091 the feces of the control and *K. pintolopesii*-colonized mice (Control, n = 4; Kp, n = 6).
1092 Bacterial load was expressed as a 2^{-Ct} value and normalized to the weight of the starting
1093 fecal material. (G) Fungal burden in the feces of GF mice after *K. pintolopesii* treatment
1094 (n = 5). (H) Scheme of fungal competition experiment in the conventional and germ-free
1095 mice. (I) Line plot of relative abundance of fungal species from ITS-marker gene
1096 sequencing of the feces at different time points in conventional and germ-free mice (n =
1097 5 per group). Dots indicate mean ± SEM. Significances were determined by unpaired two-
1098 tailed t-test. Kp, *K. pintolopesii*-colonized mice. CV, conventional mice. GF, germ-free
1099 mice

1100

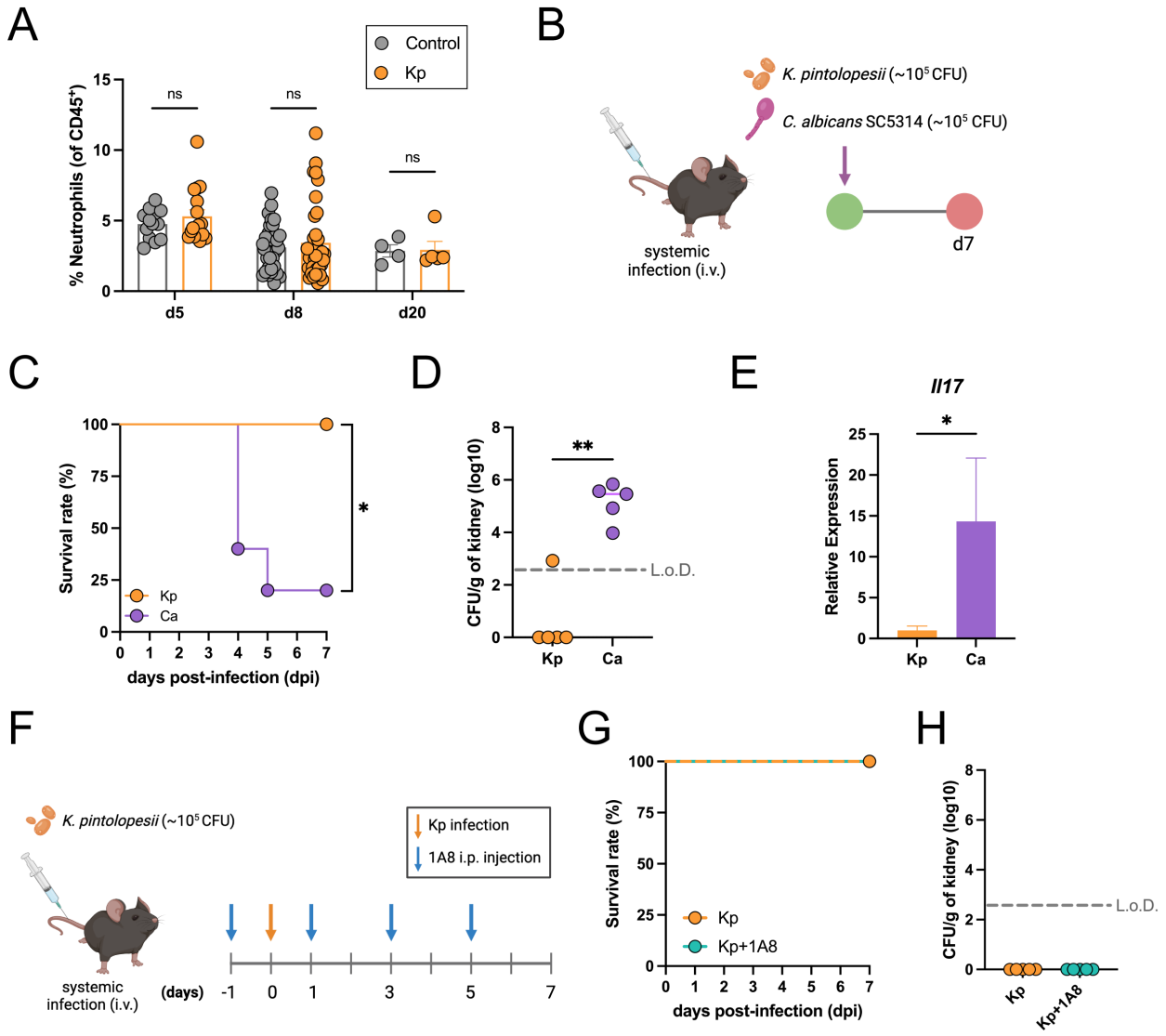

Fig. 3. The systemic challenge with *K. pintolopesii* is efficiently resolved in a neutrophil-independent manner. (A) Frequency of circulating neutrophils in the peripheral blood at 5 (Control, n = 13; Kp, n = 17), 8 (Control, n = 30; Kp, n = 35), and 20 days (Control, n = 4; Kp, n = 5) post-colonization of *K. pintolopesii*. Neutrophil populations were gated as $CD45^+$ $B220^-$ $CD11b^+$ $Ly6G^+$. (B) Scheme of the systemic challenge with *K. pintolopesii* or *C. albicans* (n = 5 per group). (C) The survival curve after *K. pintolopesii* or *C. albicans* systemic infection. Fungal burden (D) and *Il17* gene expression (E) in the

1109 kidney after *C. albicans* or *K. pintolopesii* infection. (F) Experimental schedule of
1110 neutrophils depletion and *K. pintolopesii* infection (n = 5 per group). (G) The survival curve
1111 after *K. pintolopesii* systemic infection with or without neutrophils depletion. (H) Fungal
1112 burden in the kidney after *K. pintolopesii* systemic infection with or without neutrophils
1113 depletion. Bars indicate mean ± SEM. Significances were determined by unpaired two-
1114 tailed t-test. For the survival curve, the log-rank (Mantel-Cox) test was used to find
1115 significant differences between groups. *$p < 0.05$. L.o.D., limit of detection. Kp, *K.*
1116 *pintolopesii*-colonized mice.

1117

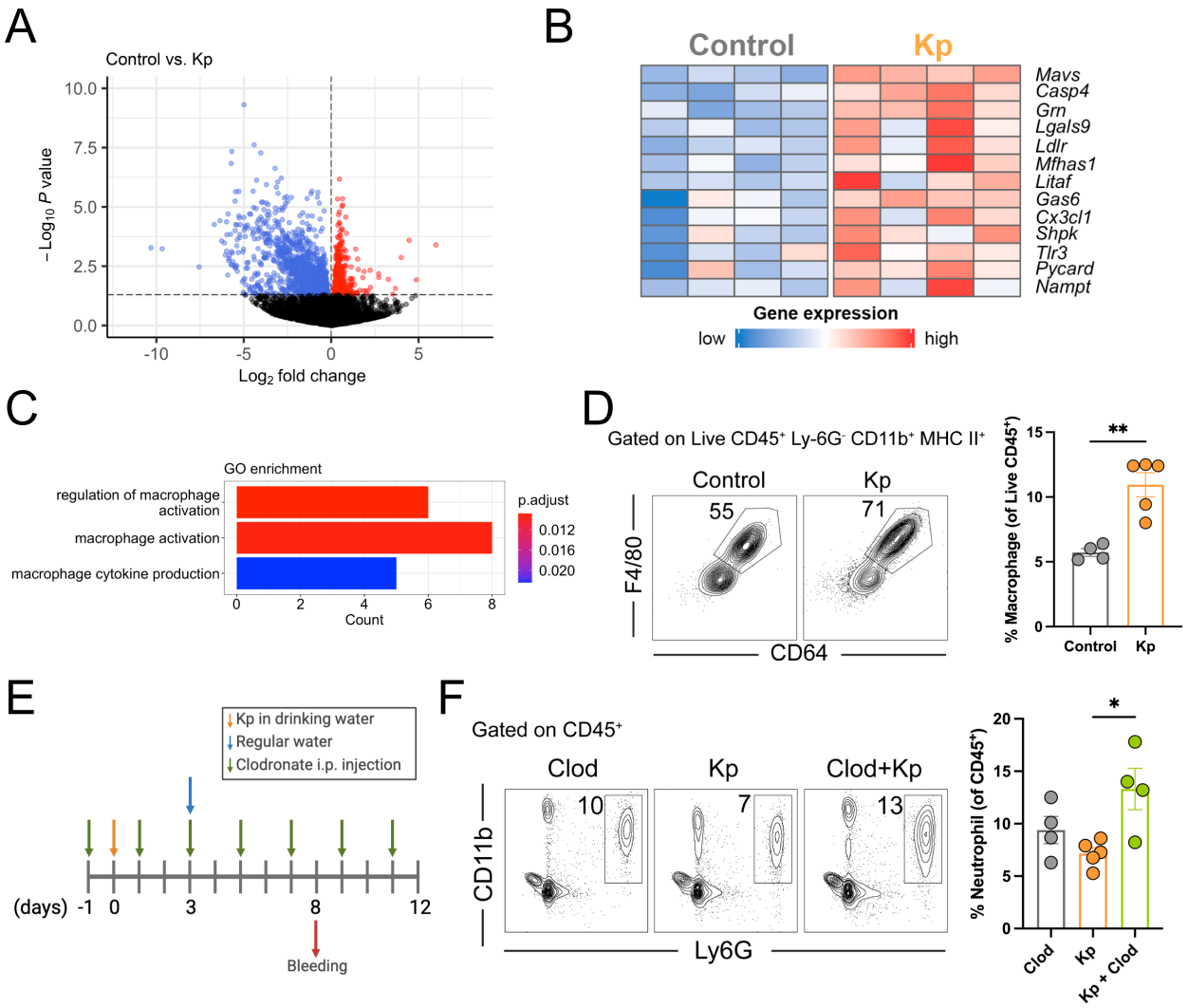

Fig. 4. *K. pintolopesii* colonization increases the macrophage population in the small intestine. (A-C) Transcriptional profiles of the small intestines from control and *K. pintolopesii*-colonized mice were generated using bulk RNA sequencing (n = 4 per group). (A) Volcano plot of the transcriptional changes after *K. pintolopesii* colonization in the small intestine. Down-regulated genes and up-regulated after *K. pintolopesii* colonization were presented as blue and red dots, respectively. (B) The heat map of macrophage activation-associated genes. (C) Bar plots from gene ontology (GO) enrichment analysis. Macrophage activation-associated terms were chosen from the list

1127 of significantly different GO terms. (D) Representative flow cytometry plots and
1128 frequency of macrophages in the small intestinal lamina propria of control and *K.*
1129 *pintolopesii*-colonized mice at 14 days post-colonization (Control, n = 4; Kp, n = 5).
1130 Macrophage populations were gated as live $CD45^+$ $Ly6G^-$ $CD11b^+$ MHC II^+ $F4/80^+$
1131 $CD64^+$. (E) Experimental schedule of clodronate injection and *K. pintolopesii*
1132 colonization. (F) Representative flow cytometry plots and frequency of neutrophils in the
1133 peripheral blood of clodronate-treated (Clod, n = 4), *K. pintolopesii*-colonized (Kp, n =
1134 5), and *K. pintolopesii*-colonized clodronate-treated mice (Kp+Clod, n = 4) at 8 days
1135 post-colonization. Neutrophil populations were gated as $CD45^+$ $B220^-$ $CD11b^+$ $Ly6G^+$.
1136 Bars indicate mean ± SEM. Significances were determined by the unpaired two-tailed t-
1137 test or One-way ANOVA with Tukey's multiple comparisons test. *$p < 0.05$ and **$p <$
1138 0.01. Kp, *K. pintolopesii*-colonized mice. Clod, clodronate-treated mice.

1139

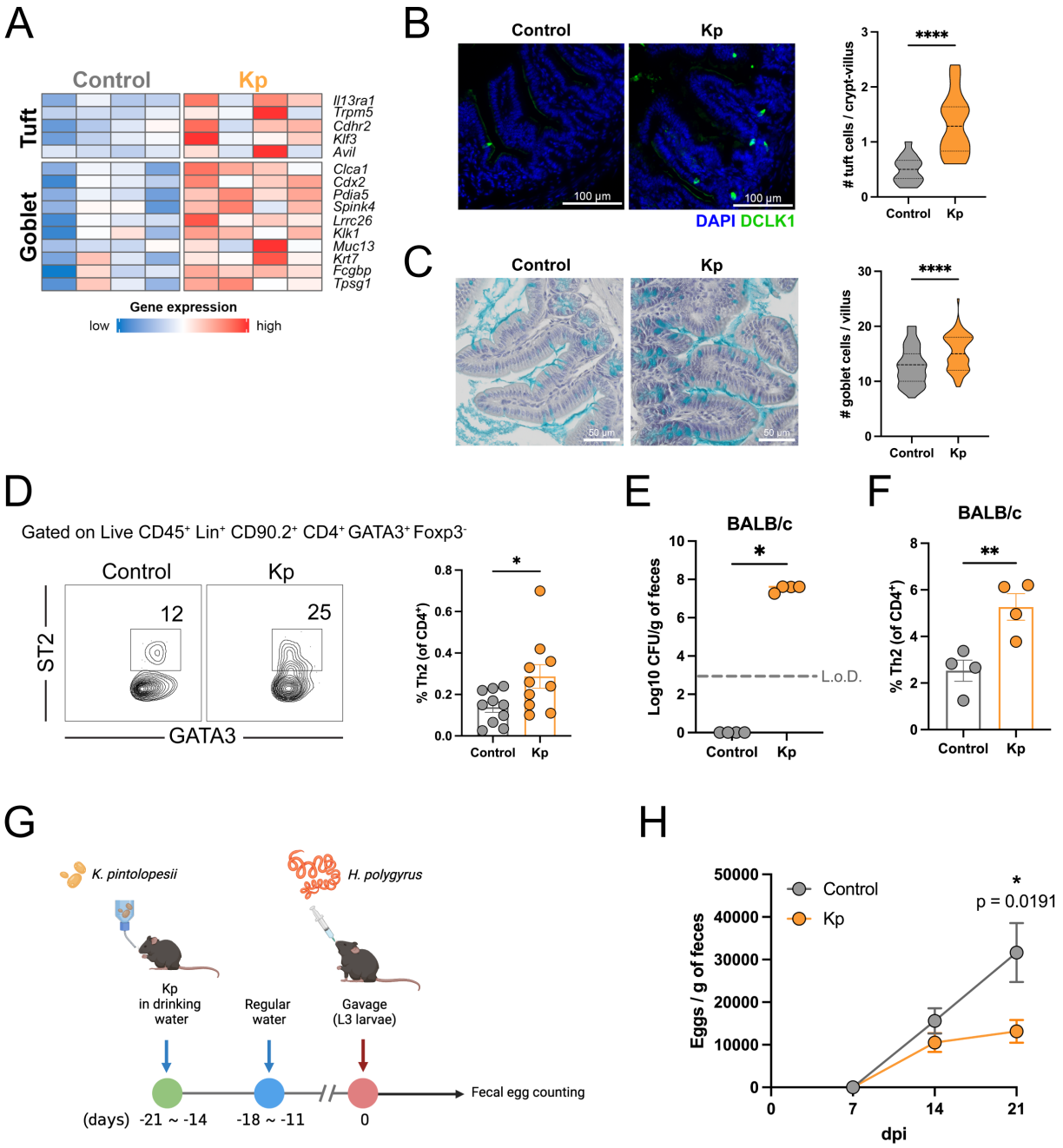

Fig. 5. *K. pintolopesii* colonization increases the tuft cell population and induces type 2 immune responses in the gut and protects the host against *H. polygyrus* infection. (A) The heat map of expression of the tuft cell and the goblet cell marker genes in the small intestine (n = 4 per group). (B) Representative image and the number of tuft cells in the small intestine of control and *K. pintolopesii*-colonized mice. Tissues were

1146 stained with DAPI (nuclei; blue) and DCLK1 (tuft cells; green). 1-7 images were used for
1147 tuft cell counting per mouse with 4–6 mice per group. (C) Representative image and the
1148 number of goblet cells in the small intestine of control and *K. pintolopesii*-colonized mice.
1149 Tissues were stained with hematoxylin (nuclei) and alcian blue (goblet cells). 6-15 villi
1150 were chosen for goblet cell counting per mouse with 4–5 mice per group. (D)
1151 Representative flow cytometry plots and frequency of Th2 in the small intestinal lamina
1152 propria of control and *K. pintolopesii*-colonized mice (n = 10 per group). Th2 populations
1153 were gated as live $CD45^+$ Lin^+ $CD90.2^+$ $CD4^+$ $GATA3^+$ $Foxp3^-$ $ST2^+$. (E) Fungal burden in
1154 the feces of BALB/c mice after *K. pintolopesii* colonization (n = 4 per group). (F)
1155 Frequency of Th2 in the small intestinal lamina propria of control and *K. pintolopesii*-
1156 colonized BALB/c mice (n = 4 per group). (G) Scheme of the *H. polygyrus* challenge. (H)
1157 The quantification of worm eggs in the feces of the control and *K. pintolopesii*-colonized
1158 mice (Control, n = 9; Kp, n = 10). Bars indicate mean ± SEM. Significances were
1159 determined by the unpaired two-tailed t-test or Mann-Whitney test. *$p < 0.05$, **$p < 0.01$,
1160 and ****$p < 0.0001$. Kp, *K. pintolopesii*-colonized mice.

1161

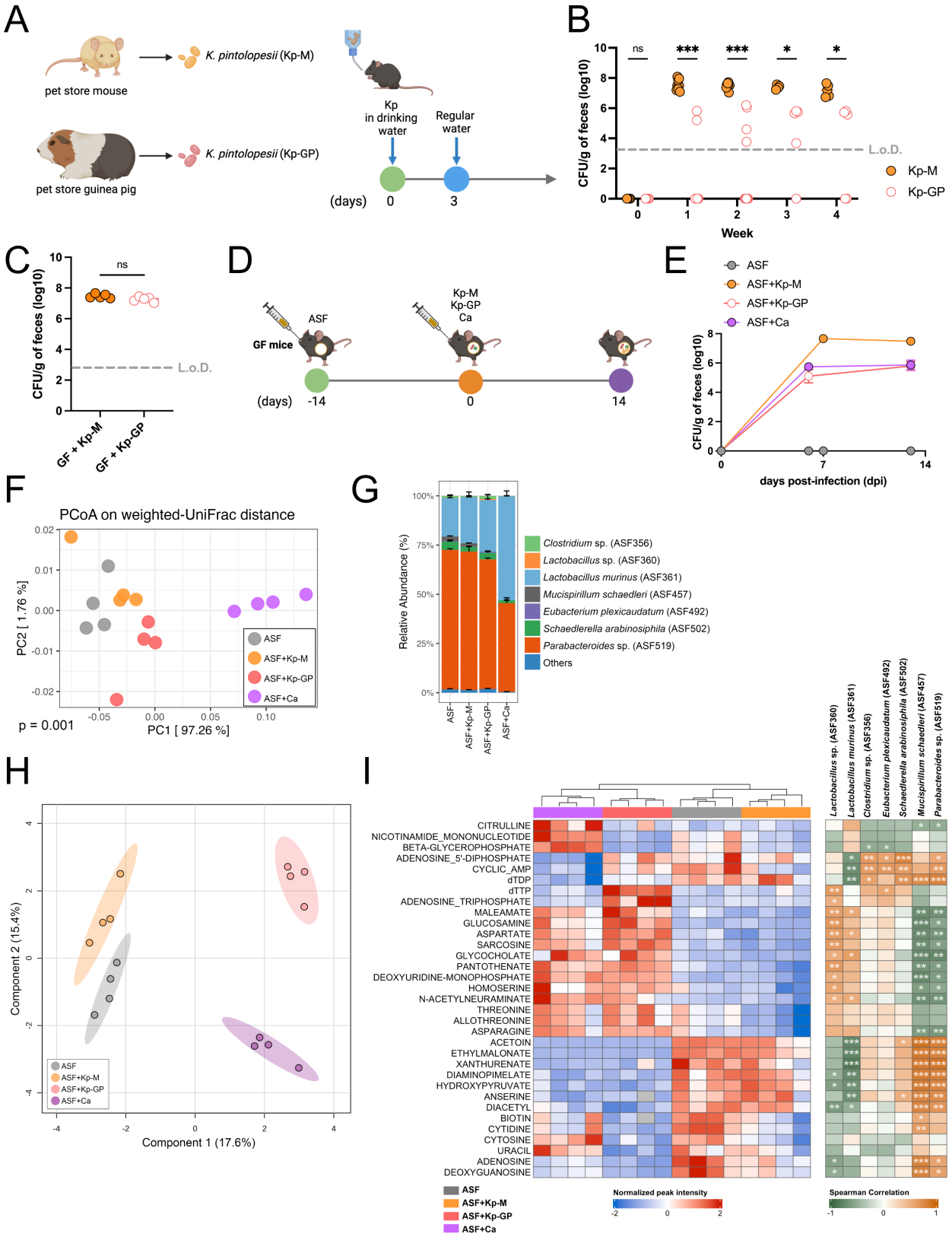
A
pet store mouse
K. pintolopesii (Kp-M)
pet store guinea pig
K. pintolopesii (Kp-GP)
Kp in drinking water
Regular water
(days) 0 3
B
CFU/g of feces (log10)
ns
***
***
*
*
L.o.D.
Kp-M
Kp-GP
Week
C
CFU/g of feces (log10)
ns
L.o.D.
GF + Kp-M
GF + Kp-GP
D
GF mice
ASF
Kp-M
Kp-GP
Ca
(days) -14 0 14
E
ASF
ASF+Kp-M
ASF+Kp-GP
ASF+Ca
CFU/g of feces (log10)
days post-infection (dpi)
F
PCoA on weighted-UniFrac distance
PC2 [1.76 %]
PC1 [97.26 %]
p = 0.001
ASF
ASF+Kp-M
ASF+Kp-GP
ASF+Ca
G
Relative Abundance (%)
Clostridium sp. (ASF356)
Lactobacillus sp. (ASF360)
Lactobacillus murinus (ASF361)
Mucispirillum schaedleri (ASF457)
Eubacterium plexicaudatum (ASF492)
Schaedlerella arabinosiphila (ASF502)
Parabacteroides sp. (ASF519)
Others
H
Component 2 (15.4%)
Component 1 (17.6%)
ASF
ASF+Kp-M
ASF+Kp-GP
ASF+Ca
I
CITRULLINE
NICOTINAMIDE_MONONUCLEOTIDE
BETA-GLYCEROPHOSPHATE
ADENOSINE_5'-DIPHOSPHATE
CYCLIC_AMP
dTDP
dTTP
ADENOSINE_TRIPHOSPHATE
MALEAMATE
GLUCOSAMINE
ASPARTATE
SARCOSINE
GLYCOCHOLATE
PANTOTHENATE
DEOXYURIDINE-MONOPHOSPHATE
HOMOSERINE
N-ACETYLNEURAMINATE
THREONINE
ALLOTHREONINE
ASPARAGINE
ACETOIN
ETHYLMALONATE
XANTHURENATE
DIAMINOPIMELATE
HYDROXYPYRUVATE
ANSERINE
DIACETYL
BIOTIN
CYTIDINE
CYTOSINE
URACIL
ADENOSINE
DEOXYGUANOSINE
Lactobacillus sp. (ASF360)
Lactobacillus murinus (ASF361)
Clostridium sp. (ASF356)
Eubacterium plexicaudatum (ASF492)
Schaedlerella arabinosiphila (ASF502)
Mucispirillum schaedleri (ASF457)
Parabacteroides sp. (ASF519)
ASF
ASF+Kp-M
ASF+Kp-GP
ASF+Ca
Normalized peak intensity
Spearman Correlation

1162

1163 **Fig. 6. *K. pintolopesii* from guinea pigs shows different characteristics in**
1164 **colonization, microbiome, metabolome, and genome compared with mouse isolate.**
1165 (A) Scheme of the colonization of *K. pintolopesii* from the pet store mouse intestine (Kp-
1166 M) and *K. pintolopesii* strain from the pet store guinea pig intestine (Kp-GP) in the
1167 laboratory conventional mice. (B) Fungal burden of Kp-M and Kp-GP in the feces at
1168 different time points. Fecal samples were collected from 4-9 mice per group at each time
1169 point. (C) Fungal burden of Kp-M and Kp-GP in the feces of germ-free mice at 14 days
1170 post-colonization (n = 5 per group). (D) Scheme of the colonization of Kp-M, Kp-GP, and
1171 *C. albicans* in the altered Schaedler flora (ASF)-colonized ex-GF mice (n = 4 per group).
1172 (E) The fungal burden of Kp-M, Kp-GP, and *C. albicans* in the ASF-colonized ex-GF mice.
1173 (F) PCoA plots based on the weighted-UniFrac distances in the feces at 14 days post-
1174 colonization in the feces of ASF mice with different strains of fungal colonization.
1175 Significances were determined by PERMANOVA. (G) Bar plot of relative abundance of
1176 ASF species from 16S rRNA gene sequencing of the feces ASF mice with different strains
1177 of fungal colonization. (H) Sparse partial least squares discriminant analysis (sPLS-DA)
1178 plot of the cecal metabolome. (I) Heatmap of the top 33 different metabolites in the cecal
1179 contents of ASF mice with different strains of fungal colonization and co-occurrence
1180 results between metabolites and bacterial abundances. Different metabolites were
1181 chosen based on the one-way ANOVA test results. Bars indicate mean ± SEM.
1182 Significances were determined by the unpaired two-tailed t-test or Mann-Whitney test. *p
1183 < 0.05 and ***p < 0.001. L.o.D., limit of detection. Kp-M, *K. pintolopesii* from the mouse-
1184 colonized mice. Kp-GP, *K. pintolopesii* from the guinea pig-colonized mice. Ca, *C.*
1185 *albicans*-colonized mice.

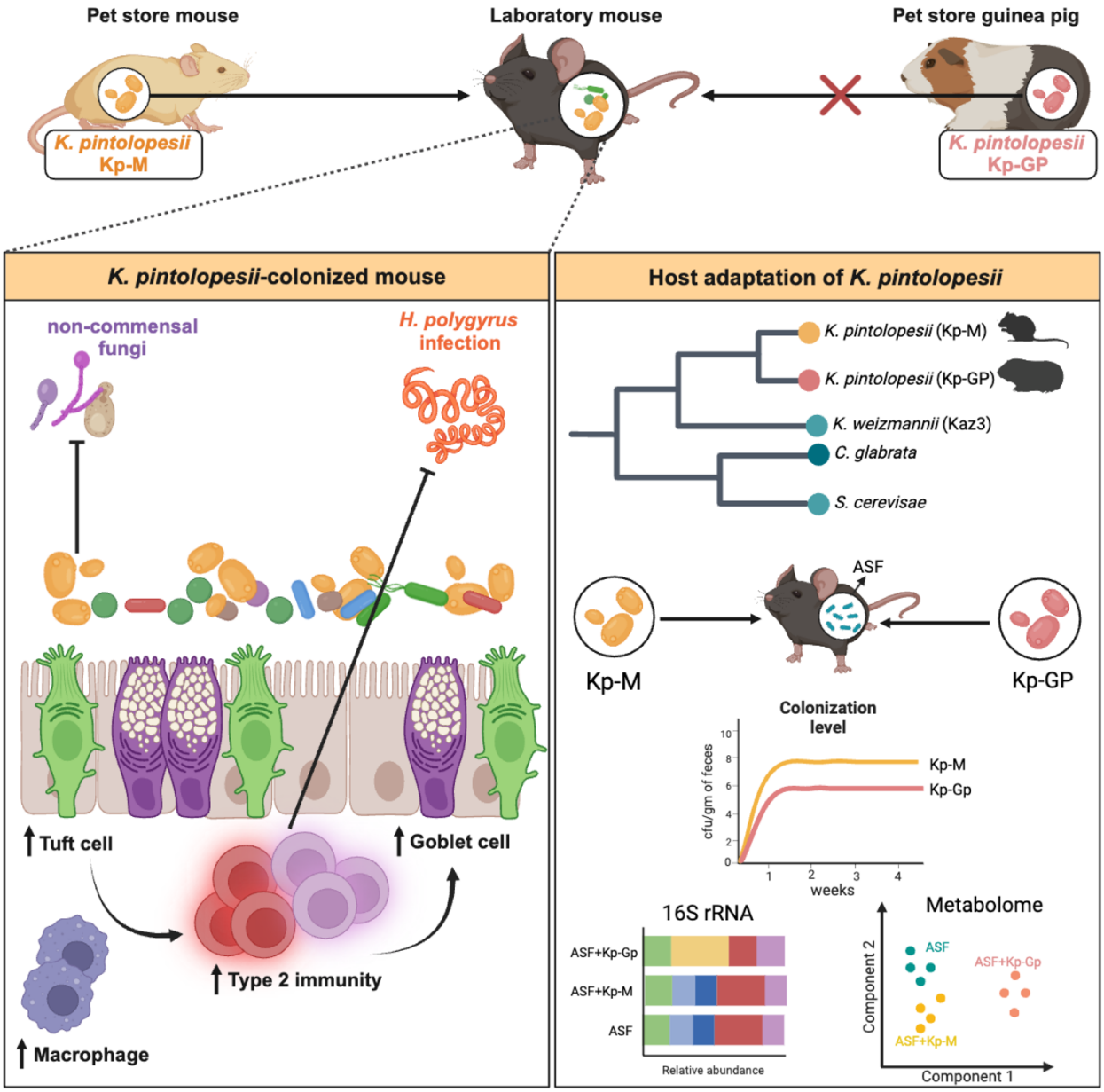

Fig. 7. Bacteria-dependent *K. pintolopesii* colonization in the mouse gut. *K. pintolopesii,* a dominant fungal species in pet store mice, stably colonizes the intestine of laboratory mice, outcompetes non-murine commensal fungi, and persists independently of gut bacteria. Its colonization expands intestinal macrophage populations, which is crucial in preventing systemic immune recognition. Additionally, *K. pintolopesii* induces type 2 immunity, conferring cross-kingdom protection against helminth infection. However,

1193 *K. pintolopesii* strains from non-murine hosts, such as guinea pigs (Kp-GP), fail to
1194 colonize laboratory mice with intact gut bacterial community despite high genomic
1195 similarity to mouse-derived strains (Kp-M). In gnotobiotic ASF mice, the Kp-GP strain
1196 disrupts bacterial communities and their associated metabolomes, a phenomenon not
1197 observed with the Kp-M strain.